Biomarker evidence for an MIS M2 glacial-pluvial in the Mojave Desert before warming and drying in the late Pliocene

Mark D. Peaple[1*], Tripti Bhattacharya[2], Jessica E. Tierney[3], Jeffrey R. Knott[4], Tim K. Lowenstein[5], Sarah J. Feakins[1]

[1]Department of Earth Sciences, University of Southern California, Los Angeles, CA 90089, USA.
[2]Department of Earth and Environmental Sciences, Syracuse University, Syracuse NY 13210, USA.
[3]Department of Geosciences, University of Arizona, Tucson, AZ 85721, USA.
[4]Department of Geological Sciences, California State University–Fullerton, Fullerton, California 92834, USA
[5]Department of Geological Sciences and Environmental Studies, State University of New York, Binghamton, New York 13902, USA
Correspondence to: M.D. Peaple, peaple@usc.edu

Key points

- Lacustrine sediments in Mojave Desert sediment core span 3.373–2.706 Ma.
- Microbial biomarkers record deep, fresh lake during cool period 3.373–3.268 Ma.
- Lake salinity increases after 3.268 Ma, associated with warming.

Abstract

Ancient lake deposits in the Mojave Desert indicate that the water cycle in this currently dry place was radically different under past climates. Here we revisit a 700 m core drilled 55 years ago from Searles Valley, California, that recovered evidence for a lacustrine phase during the late Pliocene. We update the paleomagnetic age model and extract new biomarker evidence for climatic conditions from lacustrine deposits (3.373–2.706 Ma). The MBT_{5Me}' temperature proxy, based on bacterial membrane lipids, detects present-day conditions (21 ± 3 ºC, 1σ, n = 2) initially, followed by warmer-than-present conditions (25 ± 3 ºC, n = 17) starting at 3.268 and ending at 2.734 Ma. This is supported by salinity indicators from bacterial and archaeal biomarkers that reveal lake salinity increased after 3.268 Ma. The $\delta^{13}C$ values of plant waxes (-30.7 ± 1.4‰, n = 28) are consistent with local C_3 taxa, likely expanded conifer woodlands during the pluvial with less C_4 than the

Pleistocene. δD values (-174 ± 5‰, n = 25) of plant waxes indicate precipitation δD values (-89 ± 5‰, n = 25) in the late Pliocene are within the same range as the late Pleistocene precipitation δD. Microbial biomarkers identify a deep, freshwater lake and a cooling that corresponds to the onset of major Northern Hemisphere glaciation at marine isotope stage MIS M2. A more saline lake persisted for ~0.6 Ma across the subsequent warmth of the late Pliocene before the lake desiccated at the Pleistocene intensification of Northern Hemisphere Glaciation.

Plain Language Summary

During a generally warm period three million years ago, there were large lakes in the Mojave Desert, California. We measured organic matter preserved in ancient lake mud below today's salt flat in Searles Valley to investigate the climate changes that sustained these three-million-year-old lakes. We compiled evidence for a freshwater lake, increased rainfall, and woody plants around the lake during a cooler interval, with similar-to-modern temperatures, that interrupted what was generally a warm period between five and three million years ago. Today the valley contains a saltpan, the evaporated remains of the former lake, surrounded by open desert shrubland. We compare the evidence from the lake with other climate reconstructions and find the wetter conditions coincided with cooling both locally and at higher latitudes.

1. Introduction

Multiple lines of evidence suggest that southwestern North America has become drier in recent decades and that this trend may be exacerbated by the projected further rise in CO_2 concentrations over 400 ppmv this century (Seager et al., 2007; Williams et al., 2020).

The Pliocene was the last time greenhouse gas concentrations were above 400 ppmv (Martínez-Botí et al., 2015) and the climate at that time may help contextualize current and future anthropogenic warming. The late Pliocene (Piacenzian) was the focus of PlioMIP Phase 1 (Haywood et al., 2013) and Phase 2 (Haywood et al., 2020) experiments that simulated climate during the mid-Piacenzian warm period (mPWP) between 3.264 and 3.025 Ma (De Schepper et al., 2013). Earth system models estimate global temperatures were 3.2 ºC warmer than preindustrial on average (range: 1.7–5.2 ºC), with on average 4.3 ºC warming over land and drying or modest wetting for southwestern North America (Haywood et al., 2013, 2020). The same climate models disagree about the sign of precipitation change associated with future warming in southwestern North America (Almazroui et al., 2021; Choi et al., 2016; Solomon et al., 2009).

Geological evidence for former lakes across the arid landscape of southwestern North America has long been of interest as they document wetter climate states (e.g., Russell, 1885). Lake shoreline features preserved on the landscape are typically those of the last highstand and recessional shorelines with rare examples multiple shorelines preserved (Jayko et al., 2008). In the Searles Valley basin, which includes both Searles and Indian Wells valleys, Pleistocene shorelines delineate the margins of a lake extending over 995 km^2 with a volume of 79.4 x 109 m^3 (Smith, 2009). Lake sediment cores from several valleys have revealed a continuous timeseries of fluctuations in sedimentary geochemistry, however many cores only retrieve sediments that are Pleistocene age (e.g., Smith, 1991).

Pliocene lake sediments crop out to a limited extent in several valleys east of the Sierra Nevada, California, including Death Valley (Knott et al., 2008), Searles Valley (Rittase et

al., 2020), Fish Lake Valley (Reheis et al., 1993), and Eureka Valley (Knott et al., 2019) (**Figure 1**). From this same region, Pliocene sediment cores are only available from the KM-3 core of Searles Valley (Liddicoat et al., 1980; Smith et al., 1983). Interpretation of the core sediments indicate that Searles Valley experienced several lake highstands that overflowed the sill several times since the Pliocene (Jannik et al., 1991).

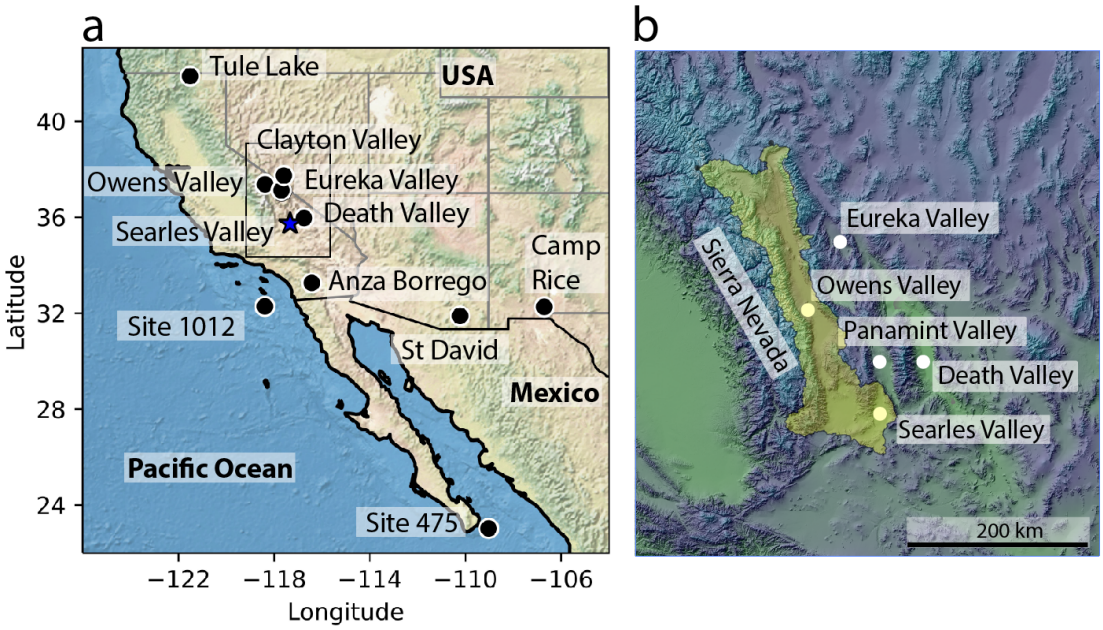

Figure 1. a) Map of southwestern North America showing Searles Lake (star) and other late Pliocene sites (circles) referred to in this study. Light grey lines represent USA state boundaries. b) Map of the western Great Basin region highlighting late Pliocene sites and the location of the Sierra Nevada (mountain range). Catchment of Pliocene Searles Valley highlighted in yellow and calculated using the 90 m Copernicus digital elevation model (European Space Agency, Sinergise 2021).

Searles Valley contains a dry lake bed with evaporite deposits spanning the Holocene, atop deposits of lake muds deposited during Pleistocene pluvials and evaporites formed during drier periods (Knott et al., 2021; Olson et al., 2023; Olson & Lowenstein, 2021; Smith, 2009). The wettest times of the last 200 ka coincided with the terminations (T2 and T1) following the last two glacial maxima of marine isotope stages (MIS) 6 and 2

(Peaple et al., 2022; Stroup et al., 2023). Plant wax δD data (Peaple et al., 2022) corroborate independent evidence from cave carbonate $\delta^{18}O$ for precipitation isotopes (Lachniet et al., 2014; Moseley et al., 2016), lending confidence to these archives of past precipitation change. Archaeal and bacterial biomarkers captured late Pleistocene evidence for changing lake salinity in Searles Lake (Peaple et al., 2021, 2022) and nearby Lake Elsinore (Feakins et al., 2019). These salinity indicators have not yet been applied to Pliocene deposits, although they were first developed in Miocene deposits (Turich & Freeman, 2011). Temperature reconstructions using bacterial lipids are more commonly applied to lake sediments and have been successfully used in Pliocene reconstructions from Lake El'gygytgyn, Siberia (Keisling et al., 2017), but not yet to any North American lacustrine deposits of Pliocene age.

In this study, we return to the late Pliocene sediments drilled from Searles Valley, previously studied for geochronology, mineralogy, and sedimentology evidence (Liddicoat et al., 1980; Smith et al., 1983) long before these biomarker methods were established. Deep drilling (~1 km) within Searles Valley reached late Pliocene deposits and identified lacustrine conditions (Smith et al., 1983), making this one of the few continuous records on land in western North America capable of resolving temporal variability within the Pliocene (Thompson, 1991). Although the late Pliocene (Piancenzian) was globally warmer, a substantial cooling event was initially described from a benthic foraminifera oxygen isotope increase in deep sea sediments (Shackleton & Opdyke, 1977). This notable glacial event is named MIS M2 based on its timing in (and below) the Mammoth subchron (3.330–3.207 Ma; Ogg, 2020). The global benthic oxygen isotope increases, Icelandic margin marine evidence for ice-rafted debris, and

glacial till in Canada, all appear in the lower Gauss subchron by 3.4 Ma (De Schepper et al., 2013), with cooling events MIS MG4 and MG2 preceeding the deeper cooling of the M2 glaciation. The MIS M2 glacial deposits at Hudson Bay indicate this glaciation was comparable in magnitude to late Pleistocene glaciations (Gao et al., 2012). The extensive Laurentide ice sheet during MIS M2 likely affected southwest climate, as ice cover has been shown to affect both winter and summer hydroclimate in the southwest (Oster et al 2015; Lora et al., 2017; Bhattacharya et al., 2018). As originally noted by Liddicoat et al., (1980) the timing of the MIS M2 glaciation coincides with a perennial lake in Searles Valley, as well as lacustrine deposition in nearby Death Valley based on outcrop studies (Knott et al., 2018).

We sampled the continuous lacustrine sedimentary sequence from Searles Valley spanning the time corresponding to the MIS M2 glaciation and the extended warmth of the mPWP. We measured branched glycerol dialkyl glycerol tetraether (brGDGT) and isoprenoidal GDGT proxies to constrain changes in air temperature and lake salinity, and plant-derived biomarkers to reconstruct the δD of precipitation. We then compared the new data for the late Pliocene to prior reconstructions of the last two glacial and interglacial cycles (Peaple et al., 2022). With a few exceptions, we were able to measure the same suite of proxies, in sediments geologically over ten times older and collected 50 years before. This new record from Searles Lake constitutes a continuous terrestrial paleoclimate sequence of the late Pliocene, yielding evidence for temperature and hydroclimate in southwestern North America for comparison to regional and global climate change.

2. Study Location

2.1. Searles Valley tectonic context

Searles Valley episodically received inflow from the eastern flank of the Sierra Nevada via the Owens River during the late Pleistocene, and the same connectivity is thought to have persisted since the Pliocene (Blackwelder, 1933; Smith, 2009; Smith et al., 1983). Tectonics and topography are important both for orographic rainfall and drainage that form lakes. The Sierra Nevada may have uplifted at a fairly steady rate from the Oligocene to the Pliocene, with high rates of incision dated to before ~3 Ma by thermochronometry (Hammond et al., 2012; McPhillips & Brandon, 2010; Stock et al., 2004), perhaps explained by high runoff during a Pliocene pluvial. Cosmogenic nuclide dating, however, puts the incision later, primarily after 2.7 Ma (Stock et al., 2004), which could allow for incision primarily by glacial scouring in the Pleistocene. Uplift continued in the Pleistocene with the fastest rates in the northern Sierra Nevada (Hammond et al., 2012). The timing of uplift matters for the leeward sedimentary archives, such as Searles Lake, because later uplift scenarios could explain a drying trend unrelated to climate change in the Pliocene. A late uplift scenario could allow up to 50% more precipitation if the mountains were 1 km lower (Smith et al., 1983). However much global evidence for recent uplift (e.g., cooling, incision) may have been conflated with late Cenozoic climatic cooling (Molnar & England, 1990) and as such fluvial or glacial erosion may well explain Plio-Pleistocene Sierra Nevada incision. The consensus from precipitation isotopes in plant wax, carbonate, and tephra hydration is that an isotopic rainshadow (D-depletion) was in place by the middle Miocene (Hren et al., 2010; Mix et al., 2016, 2019; Mulch et al., 2008). Today, such D-depleted precipitation is associated with northerly

160 moisture sources distilled by orographic processes crossing the northern and central
161 Sierra Nevada (Friedman et al., 2002).

162 Tectonics within Searles Valley and adjacent basins may have also affected Pliocene
163 basin connectivity. Lateral motion along the Marine Gate Fault (parallel to the now more
164 active Garlock Fault) resulted in several km of horizontal displacement between the
165 deposition of the lacustrine facies and their present position (Rittase et al., 2020). During
166 the Pliocene there is thought to have been some inflow from the south although the
167 catchment may not have greatly expanded. At the eastern margin of Searles Valley,
168 radiometric evidence indicates rapid exhumation of the Slate Range from 6–4 Ma
169 (Walker et al., 2014), with motion on the Searles Valley Fault (Rittase et al., 2020). The
170 deepening of the lake floor may have accompanied the uplift of the basin sides, although
171 the resulting increased accommodation space would have been counteracted by the
172 infilling of 300 m of lake sediment that accumulated between 3.4 to 2 Ma (**Figure 2**). If
173 deepening and infilling were not smoothly aligned, this may have affected the lake
174 storage capacity, and potential for spillover into downstream basins. While the
175 sedimentology of the deep Pliocene lake sediments has been interpreted as a perennial
176 lake with persistent outflow (Smith et al., 1983), geomorphological evidence is
177 inconclusive on whether outflow from Searles occurred in the Pliocene and what lake
178 depth and volume could be contained within the evolving Pliocene basin (Knott et al.,
179 2008). Although local tectonics may have had a transient influence on the potential
180 volume of Pliocene Searles Lake, large contemporaneous lakes on the regional landscape
181 robustly indicate a wet climate state (Knott et al., 2018).

2.2. Mojave Desert hydroclimate and vegetation

Today Searles Valley in the Mojave Desert has mean annual precipitation <100 mm/year, with sporadic rainfall dominantly occurring in the winter season (Western Regional Climate Center, 2022). High potential evaporation (~2,000 mm/year) in hot, dry and windy conditions means there is little to no surface water. Precipitation isotopes (δD_{precip}) reported from long-term sampling in Owens Valley (winter = -106‰, summer = -71‰), and modern groundwater in Owens Valley indicate dominantly winter recharge (Friedman et al., 1992, 2002), likely from spring melting of montane snowpack (Carrol et al., 2019). In southern Nevada, studies tracing the amount and isotopic composition of precipitation and groundwater indicate that in the lowlands too, winter precipitation contributes 90% of modern groundwater even though only 66% of precipitation occurs in winter (Winograd et al., 1998). As a result, most woody shrubs and trees across the region are deeply rooted to access consistent groundwater year-round rather than episodic rain. For example, *Juniperus osteosperma,* preferentially uses groundwater rather than summer rain (West et al., 2007). Combined ecohydrology and plant wax studies found that winter-recharge dominated groundwater is reflected in the δD of plant wax of most shrubs and trees across a coast-to-inland transect including the Mojave (Feakins and Sessions., 2010).

The vegetation of the lowlands is mostly desert shrubs with montane woodlands and forests on the Sierra Nevada. Packrat middens containing macrofossils allow for species level identification and show that *Juniperus osteosperma* woodlands expanded across the Mojave lowlands during Pleistocene pluvials (Holmgren et al., 2010; Koehler et al., 2005). Additionally, phreatophytic shrubs likely increased in Searles Valley during

glacial periods (Peaple et al., 2022) possibly exploiting elevated groundwater levels. There are no published reports of Mojave paleovegetation for the Pliocene. At coastal marine core DSDP Site 467, 400 km to the west of Searles Valley, late Pliocene pollen record similar-to-modern mixture of species including coastal oak-pine woodlands and chaparral vegetation (Ballog and Malloy, 1981; Heusser, 1981).

2.3. Sediment core and age model

We studied the Searles Lake sediment core KM-3 (USGS U234, well KM-3, 35.73371ºN, 117.32566ºW, 493 m asl) collected in 1968 by the Kerr-McGee Corporation and transferred to the US Geological Survey in 1976 (Liddicoat et al., 1980) and archived for 50 years in ambient, dry storage (USGS Core Research Center, Denver). We generated a Bayesian age model (Blaauw & Christen, 2011) for sediments from depths of 200–693 m (**Figure 2**) using previously identified paleomagnetic reversals (Liddicoat et al., 1980) and updated age estimates (Channell et al., 2020); dataset available at NOAA: Peaple et al., 2023) on the GPTS2020 timescale (Ogg, 2020).

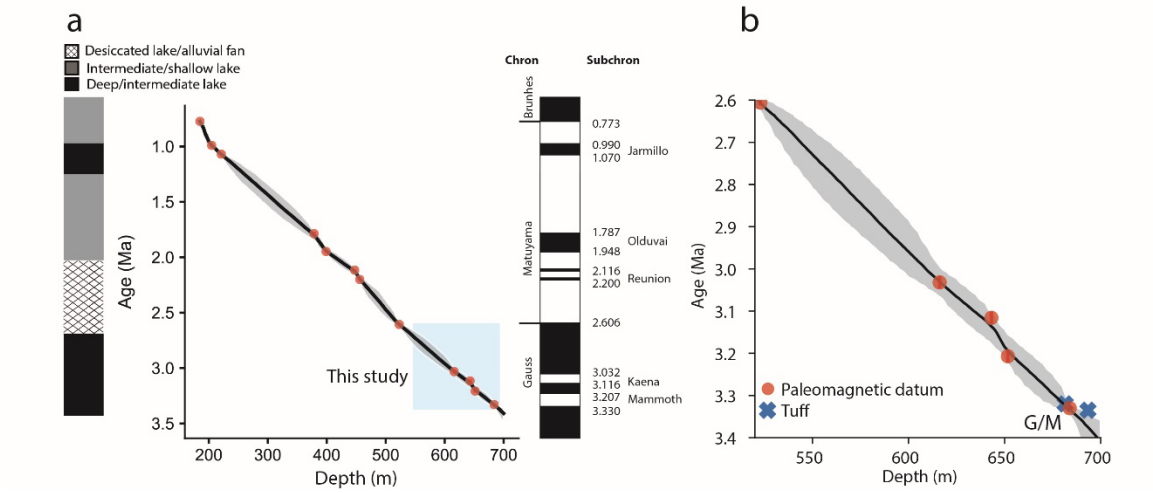

Figure 2. a) Age model generated using BACON (black line), 95% confidence interval (grey shading) and paleomagnetic datums (Liddicoat et al., 1980) updated to the

GPTS2020 (Channell et al., 2020; Ogg, 2020) (red circles). This study focused on the late Pliocene perennial lake phase (blue shading), terminating 18 m below the Gauss-Matuyama boundary (labelled G/M, 522.9 m, 2.606 Ma, 3 ka 1σ) (Liddicoat et al., 1980; Smith et al., 1983). Left: Reconstructed Searles Lake environment (Smith et al., 1983). Right: Paleomagnetic reversals. b) Section of age model covering samples in this study. Tuffs at 681.5 m and 693.4 m (blue crosses) correlate with tuffs of Mesquite Spring (3.3032 +/- 0.0025 Ma; Deino et al., 2018) and Zabriskie Wash (3.335 +/- 0.002 Ma; Knott et al., 2018) in Death Valley providing independent age constraints.

The KM-3 core contains alluvial fill deposits above bedrock (Smith et al., 1983), suggesting that tectonics of the Slate range (Walker et al., 2014) allowed for basin development and fluvial deposition before the lacustrine phase. Using our updated age model, we studied Pliocene age sediments (3.373–2.706 Ma, 693–541 m depth, **Figure 2**) comprised of grey/brown thinly bedded mudstone (Hay et al., 1991; Smith et al., 1983) previously interpreted to be deep lake facies (Unit I) representing a perennial lake (Smith et al., 1983). However, here we investigate lacustrine changes using biomarker geochemistry evidence. From 3.373–2.706 Ma, the sediments had a relatively uniform sedimentation rate (0.22 m/ka), although the Mammoth and Kaena subchrons were characterised by higher sedimentation rates (0.26 and 0.32 m/ka, respectively). The onset of lacustrine conditions has coeval timing, within Pliocene dating uncertainties, in other basins of the Mojave Desert consistent with a wetter regional climate (Knott et al., 2018). Two regionally distributed tuffs (tuffs of Mesquite Flat and Zabriskie Wash) have been correlated with tuff deposits in the KM-3 core (681.5 m and 693.4 m respectively) (Knott et al., 2018), which provide a time-equivalent marker to link the lakes in Death Valley and Searles Valley and provide a secure basis for the timing of both lakes close to the Mammoth/lower Gauss boundary at 3.330 Ma.

Four paleomagnetic age boundaries between 3.330 and 3.032 Ma make this section well-dated (1 date/100 ka) compared to the rest of core KM-3, which aids comparison to proxy syntheses and model experiments for 3.264–3.025 Ma as part of PRISM (Pliocene Research Interpretation and Synoptic Mapping), PlioMIP (Pliocene Model Intercomparison Project) and PlioMIP2 (Haywood et al., 2016). In the Searles Lake paleomagnetic chronostratigraphy, there are three paleomagnetic tie points within the PRISM/PlioMIP window: Upper Kaena or C2An.1n(o) (616.2 m, 3.032 Ma GTS2020, 7.5 ka 1σ), Lower Kaena or C2An.1r9(o) (643.1 m, 3.116 Ma, 7.5 ka 1σ) and the Upper Mammoth or C2An.2r(y) (651.7 m, 3.207 Ma, 2 ka 1σ). In sediments younger than 2.9 Ma lake elevated lake salinity is implied by the presence of the diagenetic mineral anhydrite (which replaced the evaporite mineral gypsum). Beyond the extent of this study, soils sporadically formed in the basin 2.71–2.1 Ma and after 2.1 Ma fluctuating lake levels led to interspersed deposition of evaporites and lacustrine muds (Smith et al., 1983).

3. Methods

3.1. Lipid extraction and separation

Lipids were extracted from 29 samples (~20 g) of freeze dried and homogenized sediments from core KM-3 by Accelerated Solvent Extraction (Dionex, ASE 350) using 9:1 dichloromethane (DCM):methanol (MeOH) at 100ºC and 1500 psi for 2 x 15 minute extraction cycles. Lipids were separated and purified following standard methods previously reported in detail for late Pleistocene sediments at Searles (Peaple et al., 2021). Briefly, the neutral and acid fractions were separated over aminopropyl sepra, the neutral fraction was separated into alkanes and GDGT fraction and further purified. The

acid fraction was methylated overnight in methanol of known isotopic composition with HCl to yield methyl esters and these were further separated by liquid-liquid extraction and purified by additional column chemistry prior to analysis.

3.2. Microbial biomarkers

The neutral polar fractions (containing GDGTs) were dissolved in hexane:isopropanol (99:1) and filtered through 0.45 μm polytetrafluoroethylene filters prior to analysis at the University of Arizona. GDGTs were separated using an Agilent 1260 High-Performance Liquid Chromatograph (HPLC) coupled to an Agilent 6120 mass spectrometer equipped with two Ethylene Bridged Hybrid (BEH) Hydrophilic Interaction (HILIC) silica columns (2.1 mm × 150 mm, 1.7 μm; Waters) following the method of Hopmans et al. (2016). Single Ion Monitoring (SIM) of the protonated molecules ($M + H^+$ ions) was used to detect and quantify GDGTs relative to a C_{46} internal standard (Huguet et al., 2006). Replicates were run to monitor reproducibility, to confirm that replicate precision is a trivial source of uncertainty. The largest uncertainty arises from the relative response factors between internal standard and analytes, which are unconstrained, thus concentrations should be considered semi-quantitative.

We quantified glycerol dialkyl glycerol tetraether (GDGTs), including the branched (br) GDGTs, derived from bacterial membrane lipids, and the isoprenoid (isoGDGTs) derived from archaea. In addition to the concentration of individual compounds and summed totals (Σ) for each compound class, we calculate ratios that are informative about aspects of microbial production and limnological conditions. The relative abundance of individual compounds can be useful as indicators of microbial community and limnologic conditions. Crenarchaeol (cren) is produced uniquely by Thaumarchaeota (e.g.,

Sinninghe Damsté et al., 2002; Schouten et al., 2013), often dominant in oxic lakes (Baxter et al., 2021). While caldarchaeol (GDGT-0) is also produced by Thaumarcheota (e.g., Sinninghe Damsté et al., 2012b; Schouten et al., 2013), GDGT-0 without crenarchaeol implies water column anoxia and other producers including anaerobic methane-oxidizing archaea (Pancost et al., 2001; Schouten et al., 2001) and methanogenic Euryarchaeota (Schouten et al., 2013, and references therein). We report the proportion of GDGT-0 to inform on lake stratification and anoxia, simply calculated relative to summed isoGDGTs as follows:

$$\mathrm{f(GDGT-0)} = \frac{[\mathrm{GDGT-0}]}{\Sigma \mathrm{isoGDGT}}\ x\ 100 \quad (1)$$

We calculate the archaeol caldarchaeol ecometric (ACE), a salinity index (Turich and Freeman, 2011), where:

$$\mathrm{ACE} = \frac{[archaeol]}{[archaeol]+[\mathrm{GDGT-0}]}\ x\ 100 \quad (2)$$

As archaeol is dominantly produced by halophilic archaea a higher ACE index is interpreted to represent more saline lake conditions (Turich and Freeman, 2011).

For the bacterial brGDGTs, the numbers I, II, and III refer to brGDGTs with four, five, and six methyl groups, and a, b, and c include zero, one, and two rings, respectively, the one two and three prime symbols (′) denote structural isomers with the methyl group at different positions. We calculate $IR_{6+7Me,}$ an index sensitive to changes in lake salinity (H. Wang 2021)

$$IR_{6+7Me} = \left[\frac{IIa'+IIb'+IIc'+IIIa'+IIIb'+IIIc'}{IIa+IIb+IIc+IIIa+IIIb+IIIc+IIa'+IIb'+IIc'+IIIa'+IIIb'+IIIc'} + \frac{IIIa'''+IIa'''}{IIIa+IIIa'+IIIa'''+IIa+IIa'+IIa'''}\right] \times 0.5 \quad (3)$$

315 The temperature-sensitive MBT'_{5Me} index is the relative methylation of the 5′ methyl
316 brGDGTs, where:

317 $$MBT'_{5Me} = \frac{[Ia+Ib+Ic]}{[Ia+Ib+Ic+IIa+IIb+IIc+IIIa]} \quad (4)$$

318 We use the Bayesian $BayMBT_0$ calibration of a global lake dataset (Martínez-Sosa et al.,
319 2021) to convert MBT'_{5Me} to the mean temperature of the months above freezing.

320 3.3. Plant wax biomarkers

321 The plant wax-derived *n*-alkanoic acids (analyzed as methyl esters from C_{16} to C_{32} carbon
322 chain length), were quantified using an Agilent Gas Chromatograph Mass Spectrometer
323 (GC-MS). We report concentrations for the individual *n*-alkanoic acids and compute the
324 summed C_{22}-C_{32} *n*-alkanoic acid concentrations (Σalkanoic acid abundance) as well as
325 carbon preference index (CPI) and the average chain length (ACL) calculated as:

326 $$\mathrm{CPI} = \frac{2[\mathrm{C_n}]}{[\mathrm{C_{n-1}}]+[\mathrm{C_{n+1}}]} \quad (5)$$

327 $$\mathrm{ACL} = \sum(\mathrm{n} \times [\mathrm{C_n}]) \sum[\mathrm{C_n}] \quad (6)$$

328 where the chain length (n) refers to the C_{22} to C_{32} *n*-alkanoic acids.

329 The *n*-alkanoic acid methyl esters were analyzed by Thermo GC equipped with a Triplus
330 autosampler and a 30 m column (0.25 mm internal diameter, with a 0.25 μm type 5
331 coating) coupled via an Isolink (1000/1400ºC) for combustion or pyrolysis and Conflo IV
332 to an isotope ratio mass spectrometer (GC-IRMS) and analyzed for C and H isotopic
333 composition. Samples were injected with bracketing CO_2 and H_2 reference gases for
334 comparison between sample and standard runs. Normalization of measured $\delta^{13}C$ and δD
335 values to the international reference standards Vienna Standard Mean Ocean Water and
336 Vienna Pee Dee Belemnite respectively was achieved with a multi-point organic

reference standard containing C_{16}-C_{30} *n*-alkanes of known isotopic compositions (A6 mix supplied by A. Schimmelmann, University of Indiana; $\delta^{13}C$ values from −25.9 to −33.7‰ and δD values from −17 to −256‰). The RMS uncertainty for measured to known standard values for $\delta^{13}C$ and δD analyses was better 0.1‰ and 5‰ respectively. Replicate sample analyses indicate have on average 0.03‰ and 2‰ instrument precision. Linearity was assessed daily across 1–8 V, for $\delta^{13}C$ (σ = 0.07‰), and for δD the linearity is applied as a correction (H_3^+ factor averaged 9.89 ppm/mV) the latter applied as a correction within Isodat. Reported $\delta^{13}C$ and δD values for *n*-alkanoic acids were corrected to account for the contribution of the methyl group (Lee et al., 2017).

Plant wax $\delta^{13}C$ and δD values were used to reconstruct vegetation and precipitation isotopic composition similar to previous applications to the late Pleistocene Searles Lake core studying both the *n*-alkanoic acids and *n*-alkanes (Peaple et al., 2022) and regional applications for the Pleistocene (Bhattacharya et al., 2018; Feakins et al., 2019) and Pliocene (Bhattacharya et al., 2022) all performed on *n*-alkanoic acids. The δD value of precipitation was reconstructed from the δD value of C_{28} and C_{30} *n*-alkanoic acids by applying a regional $\varepsilon_{wax/precip}$ of -93‰ (Feakins et al., 2014, 2019; Feakins & Sessions, 2010), where:

$$\delta D_{precip} = \frac{\delta D_{wax} + 1}{\varepsilon_{wax/precip} + 1} - 1 \quad (7)$$

A constant fractionation is appropriate as no gradient was observed across the modern climatic gradients in the region (Feakins and Sessions, 2010) and pollen-adjusted $\varepsilon_{wax/precip}$ had minimal effect within the Pleistocene (Peaple et al., 2022).

The *n*-alkane fraction contains an uncharacterized complex mixture indicating a mature hydrocarbon contribution from degradation in situ, sedimentary migration of petrogenic hydrocarbons or contamination during drilling. The dominance of mature hydrocarbons in Pliocene sediments from KM-3 precludes consideration of plant wax *n*-alkanes, which has been the preferred plant wax precipitation isotope indicator in the late Pleistocene sediments (Peaple et al., 2022).

3.4. Pollen

Following standard pollen methodology as in a study of the late Pleistocene in this basin, we screened 1cc of sediment from two initial samples selected at random from the 29 samples studied for biomarkers. While pollen was well-preserved in late Pleistocene sediments drilled in 2017 (Peaple et al., 2022), Pliocene-age samples from core KM-3 were barren of pollen. We have since learnt that pollen was not found in initial surveys of the KM-3 core in 1976 as well during a second attempt in the late 1990s. We thus conclude core storage is not the issue, but rather degradation in situ in the last 3 Ma. We report the null result to save additional fruitless effort at palynology.

3.5. Statistics

3.5.1. Breakpoint analysis

We used the offline Power of the Pruned Exact Linear Time (PELT) (Wambui et al., 2015) method implemented in the Ruptures Python library (Truong et al., 2020). PELT is an exact search algorithm that uses a least squares deviation cost function to detect mean changes (changepoints) in our time series.

3.5.2. Intergroup differences

In order to determine if there are statistically significant differences between groups of samples, we used a two-sided non-parametric Kolmogorov-Smirnov test. Taking into account age uncertainty, we calculated the p value for the Kolmogorov-Smirnov for each Bacon age ensemble member to generate a distribution of p values. We then calculated the median p value of this distribution to establish whether groups are statistically different ($p < 0.05$).

4. Results

We present the biomarker results for the late Pliocene lacustrine deposits from the KM-3 core at Searles Lake (**Figure 3**) in the context of the limnological interpretation of Smith et al., (1983) (**Figure 3a**).

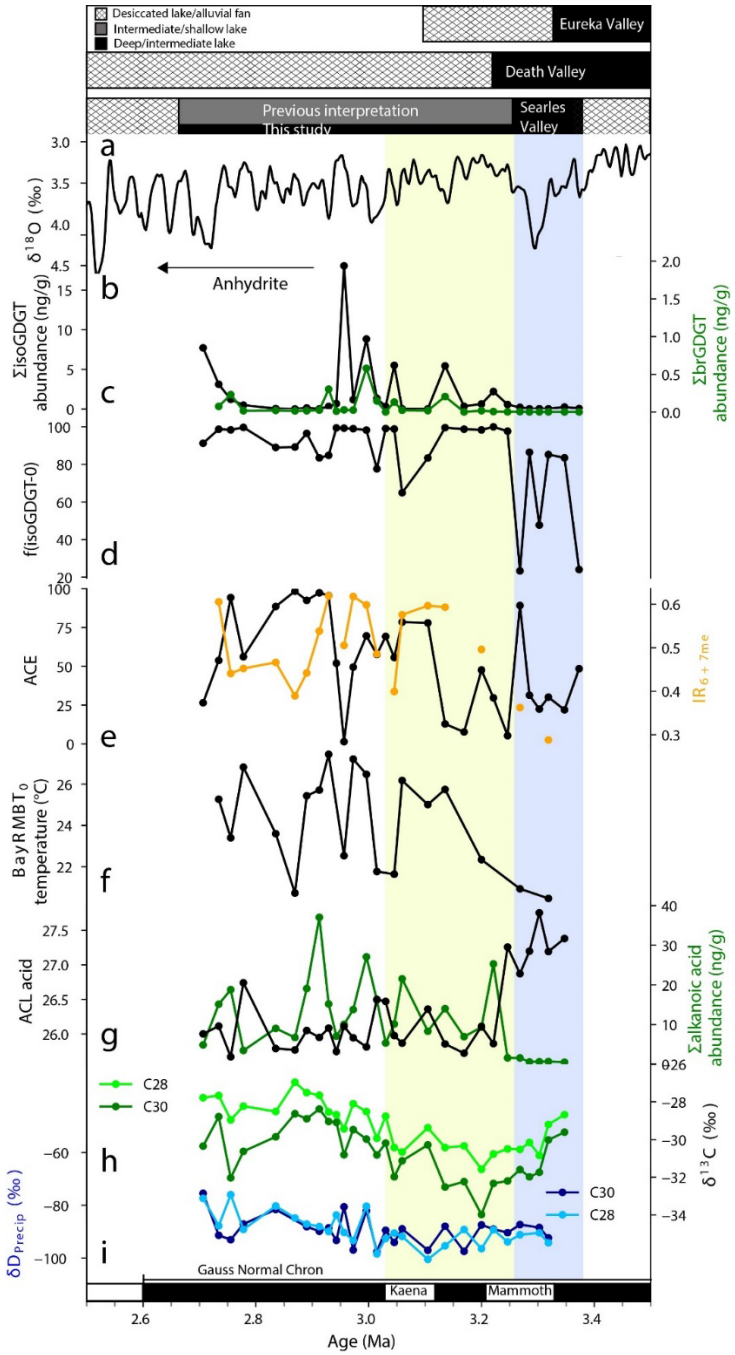

Figure 3. Searles Lake proxy reconstructions for the Late Pliocene. Comparison of a) summary of lake depth from Eureka Valley's Lake Andrei (Knott et al., 2019), Death Valley (Knott et al., 2018) and Searles Lake (Smith et al., 1983). b) Global composite record of benthic foraminiferal carbonate $\delta^{18}O$ binned, resampled and smoothed with a locally weighted function to 20 ka resolution (Westerhold et al., 2020). Searles Lake proxy reconstructions from core KM-3 (this study) including: c) ∑brGDGT and ∑isoGDGT concentrations (note different axes) c) proportion of isoGDGT-0 an indicator of stratification and anoxia, e) ACE and IR_{6+7Me} indices of salinity, f) $BayMBT_0$ temperature reconstruction of mean air temperature for months above freezing, g) $\sum C_{22-32}$ alkanoic acid concentration and Average chain length (ACL) of *n*-alkanoic acids, h) $\delta^{13}C$ value of C_{28} *n*-alkanoic acid (light green) and C_{30} *n*-alkanoic acid (dark green), and i) δD value of precipitation (light and dark blue as for h). Blue shading represents Searles Lake deep lake period (3.373–3.268 Ma) overlapping with the Mammoth reverse chron. Yellow shading represents the mid-Pliocene warm period (3.264–3.025 Ma). Paleomagnetic age boundaries are shown on the x axis.

4.1. GDGTs

4.1.1. Concentrations

ΣisoGDGTs (2.01 ± 3.86 ng/g, n = 29) far exceed the concentrations of ΣbrGDGTs (0.07 ± 0.13 ng/g, n = 29) (**Figure 3c**), showing dominance of archaeal rather than bacterial production. Downcore spikes in abundance in both compound classes could be due to production, preservation or most likely reduced sedimentary dilution. While GDGTs were measured on all 29 samples, some compounds, especially some of the brGDGTs and cren, were too low abundance to be identified in all samples, limiting availability of some of the derived indices.

4.1.2. Stratification indicators

GDGT-0 (caldarchaeol) is the dominant isoGDGT (83 ± 23%, n=29; **Figure 4**), suggesting that methanogenic archaea dominated (Schouten et al., 2013) under a stratified water column with low dissolved oxygen concentrations. GDGT-0 has a lower proportional abundance (57.3 ± 32.8%, n = 22) before 3.221 Ma indicating a modest amount of mixing and oxygenation and some other archaeal production compared to the

421 remainder of the record when GDGT-0 dominates (90.6 ± 12.3%, n= 7). Cren (and its
422 isomer) have very low concentrations (cren averages 0.5%, and cren′ 0.2%) suggesting
423 that conditions were rarely favorable for Thaumarchaeota, and that the lake remained
424 dominantly stratified and anoxic in the late Pliocene (**Figure 4**).

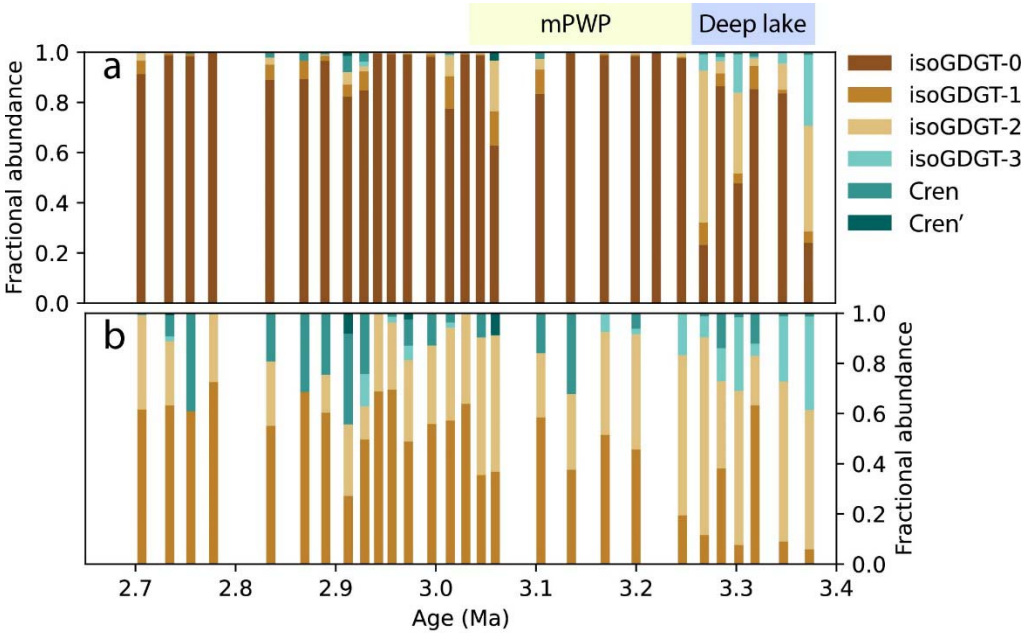

425
426 **Figure 4**. a) Fractional abundance of isoGDGTs through time. b) Fractional abundance of
427 isoGDGTs without isoGDGT-0. Labels for mPWP and deep lake as for Figure 3.

428 4.1.3. Salinity indicators

429 Both salinity indicators are low from 3.373–3.268 Ma (**Figure 3e**) with ACE (40.6 ±
430 17.6%, n = 6) and IR_{6+7Me} (0.33 ± 0.04, n = 2) denoting lower salinities and fresh to
431 brackish conditions. Higher ACE (57.3 ± 6.5%, n = 23) and IR_{6+7Me} (0.52 ± 0.02, n = 17)
432 indicate saline conditions, including hypersalinity, from 3.268 to 2.706 Ma. In order to
433 statistically evaluate if there are salinity differences between these two periods across
434 both proxies, we calculated a two-sided Kolmogorov-Smirnov test for each age ensemble
435 member generated from Bacon and then calculated the median p value from this
436 ensemble. The median p values from the resultant p value ensembles for ACE and

437 IR_{6+7Me} (0.033 and 0.012) indicate that the salinity differences for these two intervals are
438 statistically significant for both indicators, one bacterial, one archaeal, providing robust
439 evidence for the salinity change.

440 4.1.4. Temperature proxies

441 MBT'_{5Me} indicates temperatures of 20 to 30 °C from 3.319 to 2.706 Ma using the
442 $BayMBT_0$ lakes calibration (MAF, months above freezing) (Martínez-Sosa et al., 2021)
443 (**Figure 3f**). Low concentrations of brGDGTs, limit the detection of the minor GDGT
444 compounds needed to calculate the bacterial temperature index especially in the early part
445 of the record. This may be because of low bacterial production or subsequent
446 degradation. Although the data are sparse, the first two temperature estimates, dated to
447 3.319 and 3.268 Ma, yielded a mean temperature of 21 ± 3°C (compound 1σ uncertainty,
448 n = 2), followed by a warming of 4 °C after 3.268 Ma to a mean temperature of 25 ± 3 °C
449 (n =17) across 3.246–2.734 Ma. The temperatures from these periods are significantly
450 different following our age uncertain Kolmogorov-Smirnov approach (Section 3.4.3).

451 4.2. Plant wax

452 4.2.1. Concentrations

453 Summed *n*-alkanoic acid (C_{22}-C_{32}) concentrations (Σalkanoic acid) averaged 11.0 ± 9.2
454 ng/g (n = 28). Σalkanoic acid concentrations are low (0.9 ± 0.5 ng/g, n = 6) before 3.221
455 Ma, thereafter, increasing to higher concentrations (13.8 ± 8.4 ng/g, n = 22) (**Figure 3g**).
456 Visual inspection of smear slides showed a shift from coarser grains (sand) to finer
457 grained (silt/clay) lithology at 3.221 Ma. Although not a quantitative comparison, coarse
458 grained materials result in volumetric dilution of biomarkers, whereas fine-grains provide
459 more surface area for the preservation of organic matter. The carbon preference index

460 (CPI) was consistently low (3.3 ± 0.3, n = 28). The average chain length (ACL) of the
461 C_{22}-C_{32} alkanoic acids was slightly longer (27.4 ± 0.3, n = 4) before 3.268 Ma than after
462 (26.1 ± 0.4, n = 24) thereafter; overall (26.3 ± 0.6, 1σ, n = 28). Reduced ACL after 3.268
463 Ma may reflect a shift in aquatic macrophyte production or the terrestrial plant
464 community (Peaple et al., 2021) and/or may suggest more microbial degradation in soils
465 (Brittingham et al., 2017; M. S. Wu et al., 2019) during the warmer and drier climate.

466 4.2.2. Carbon isotopic composition

467 $\delta^{13}C$ values for the C_{28} *n*-alkanoic acids range from -31.6 to -27.0‰ (-29.2 ± 1.2‰, n =
468 28) and for the C_{30} *n*-alkanoic acids -34.0 to -28.4‰ (-30.7 ± 1.4‰, n = 28) (**Figure 3h**).
469 The $\delta^{13}C$ values of the C_{30} *n*-alkanoic acids range from a high of -29.6‰ at 3.478 Ma, to
470 a low of -34.0‰ at 3.200 Ma and then return to generally high values from 3.0-2.7 Ma
471 with a high of -28.4‰ at 2.891 Ma.

472 4.2.3. Hydrogen isotopic composition

473 The δD values of the C_{28} *n*-alkanoic acids (-174 ± 6‰, n = 26) and the C_{30} *n*-alkanoic
474 acids (-174 ± 5‰, n = 25), are the same within uncertainty, however the individual
475 samples show variable offsets for the C_{28}-C_{30} (+10 to -17‰), perhaps source differences,
476 or analytical noise. Applying the $\varepsilon_{wax/precip}$ regionally defined fractionation for plant wax
477 *n*-alkanoic acids (Feakins et al., 2014, 2019), the measured δD values for C_{28} yield
478 precipitation isotopic composition (δD_{precip}) estimates for the Pliocene interval (-89 ±
479 6‰, n = 26) and values calculated from C_{30} are equivalent (-89 ± 5‰, n = 25). Downcore
480 variations of 22‰ (**Figure 3h**) do not covary with plant wax $\delta^{13}C$ or abundance
481 distributions so appear robust to plant type and preservation, they may carry signals of
482 hydroclimate or heterogeneous catchment erosional inputs.

5. Discussion

5.1. Lake depth reconstruction

Lake depth in terminal lakes is inversely related to water salinity, as evaporation leaves behind the salts delivered by river inflow. Smith et al. (1983) originally depicted lacustrine sedimentation as evidence for a consistently deep lake from 3.4 to 2.6 Ma (dates updated to the current timescale; **Figure 3a**). However, this was apparently a simplification as they also described the presence of the diagenetic mineral anhydrite (which replaced gypsum) at depths of 681.8 to 546.2 m, indicating the precipitation of evaporite minerals in sediments younger than 2.9 Ma (**Figure 3a**), which implies saline lake conditions. Anhydrite-rich sandstones, indicating saline waters, were also reported by Hay & Guldman (1987) at depths of 656.6 to 640.2 m. We report new biomarker evidence for saline lake waters (**Figure 3e**) that lead to a revised interpretation (**Figure 3a**) consistent with adjacent lake basins. We present biomarker-based salinity reconstructions derived from different microbial lineages: the ACE and the IR_{6+7Me} salinity proxies are calculated from the lipids of archaea and bacteria respectively, known for detection of hypersaline and brackish water lakes respectively (Turich and Freeman, 2011; H. Wang et al., 2021) and applied to Pleistocene salinity variations in this lake basin (Peaple et al., 2022). While the bacterial and archaeal communities are unknown for the (former) Searles Lake, each has their own salinity tolerance ranges and environmental sensitivities, based on paleoenvironmental comparisons in the Pleistocene sediments in the SLAPP-SRLS17 core (Peaple et al., 2022) and sampling of modern conditions in Asian lakes (H. Wang et al., 2021). Here, during the cool-temperature phase (**Figures 5a-e**) both ACE and IR_{6+7Me} proxies (**Figures f-g**) are low consistent with lower

506 salinity and brackish, perennial lake conditions. We detect increases in the IR_{6+7Me} at
507 3.268 Ma and this coincides with local warming detected by $BayMBT_0$ (**Figure 5e**) and
508 global warming into the late Pliocene warm period (**Figure 5a and b**). The ACE salinity
509 index has a step change increase after 3.14 Ma (**Figure 5f**), which lags the change
510 observed in the IR_{6+7Me} record (**Figure 5g**) possibly due to the low sensitivity of ACE at
511 low salinities (Peaple et al., 2022; H. Wang et al., 2021). The dual archaeal and bacterial
512 biomarker evidence for increasing salinity reported here, together with the preservation of
513 anhydrite noted by Smith et al., (1983), each provide independent confirmation for a
514 saline lake during the mPWP.

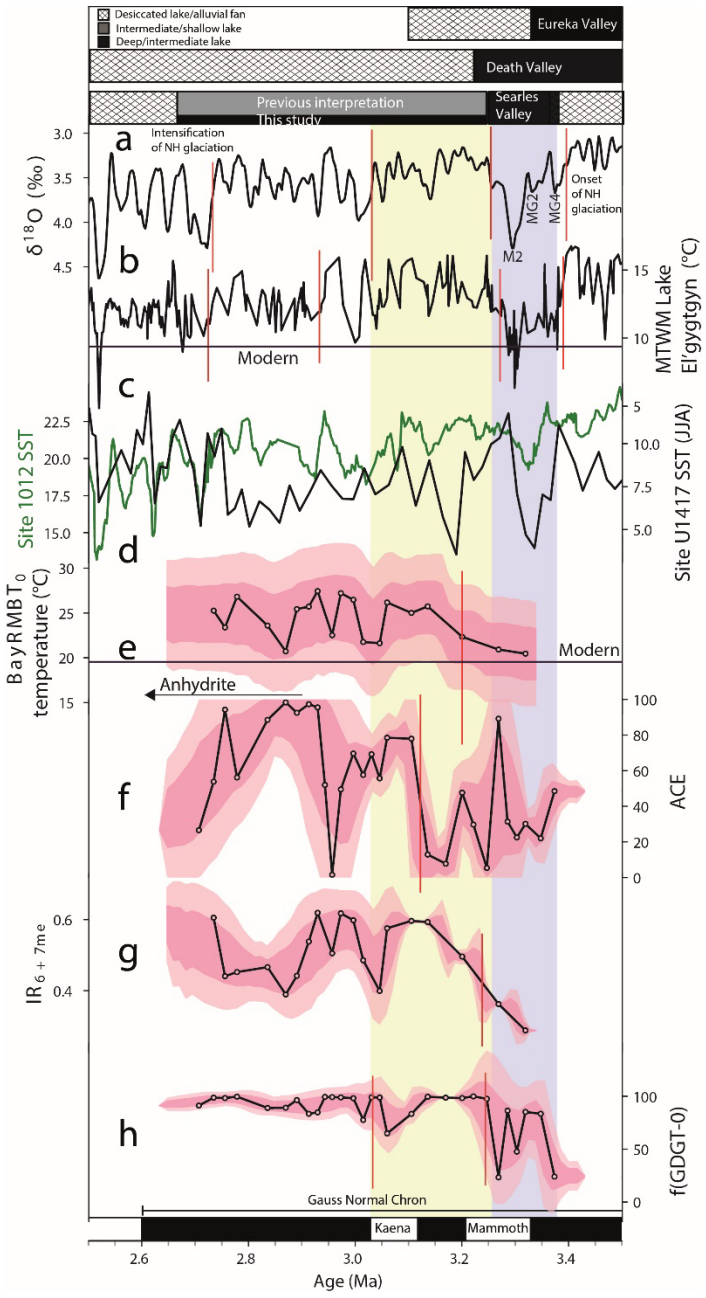

515

516 **Figure 5.** Global and regional context for comparison to Searles Lake GDGT proxy
517 reconstructions for the Late Pliocene. a) Summary of Eureka Valley, Death Valley and
518 Searles Valley paleoenvironments. b) Global composite record of benthic foraminiferal
519 carbonate $\delta^{18}O$ binned, resampled and smoothed with a locally weighted function to 20
520 ka resolution (Westerhold et al., 2020). Annotated with the names of the MIS MG4, MG2
521 and M2 glacial events. c) Lake El'gygtgyn, Siberia, mean temperature of warmest month
522 (MTWM) reconstructed from pollen compared to modern (Brigham-Grette et al., 2013).
523 d) Sea surface temperatures (SSTs) from alkenone Uk'_{37} index in the Gulf of Alaska
524 (Sánchez-Montes et al., 2020) and ODP 1012 (Brierley et al., 2009) recalibrated using

BAYSPLINE (Tierney & Tingley, 2018). Select Searles Lake proxy reconstructions from core KM-3 (this study) including: e) $BayMBT_0$ temperature reconstruction of mean air temperature for months above freezing (MAF) compared to modern (dashed line), f) ACE index of salinity g) IR_{6+7Me} index of salinity, and h) f(GDGT-0) index. Change points (red lines) calculated using the Pruned Extract Linear Time algorithm using the Ruptures python package (Truong et al., 2020). Shading and age control as in Figure 3.

Corroborating evidence for the transition from a deep freshwater lake to a shallow, saline lake comes from other isoGDGTs. Methanogenic archaea should flourish under expanded anoxic conditions in the water column (Besseling et al., 2018; Blaga et al., 2009; Qian et al., 2019; Schouten et al., 2002), with f(GDGT-0) >90% associated with dissolved oxygen <0.8 mg/L environments in a modern lake water profile study (J. Wu et al., 2021). GDGT-0 can also be produced in anoxic lake floor sediments (Blaga et al., 2009) by methanogenic archaea, with increases in the proportion of the GDGT-0/cren ratio occurring in the top 5 cm of sediment (Blaga et al., 2009). In these Pliocene lacustrine muds, we find that f(GDGT-0) is reduced (57.3 ± 32.8%, n = 7) between 3.373 to 3.246 Ma (**Figure 3d**), suggesting that parts of the lake system were relatively more oxygenated during what we infer to be a deep lake. In contrast, we find higher f(GDGT-0) later in the record (90.6 ± 11.2%, n = 22) in what we infer to be a shallower, more stratified and stagnant lake. Similarly, high f(GDGT-0) has been associated with shallower lake phases in mid-latitude Asian lakes and Tibetan Plateau lakes (Li et al., 2023). The proportion of GDGT-2 expands during the shallow, stratified lake period between 3.373 to 3.246 Ma (19.4 ± 18.7%, n=7; **Figure 4**). Production of GDGT-2 at depth in stratified lakes has been linked to deep dwelling Thaumarcheota (Baxter et al., 2021; Zheng et al., 2022) as well as in-sediment production (Sinninghe Damsté et al., 2012). An increase in the proportion of GDGT-2 was also identified in the Great Salt Lake, USA following a transition from more saline and shallower to fresher and deeper lake phases in Holocene

551 sediments (So et al., 2022). Thus, the high %GDGT-2 and relatively low %GDGT-0,
552 together with low salinity, support a deep stratified lake between 3.373 to 3.246 Ma. The
553 presence of a lake in nearby Death Valley between 3.5 and 3.3 Ma (Knott et al., 2018),
554 supports the interpretation of pluvial conditions in Searles Valley between 3.373 to 3.246
555 Ma. Conversely from 3.221 to 2.706 Ma, isoGDGTs were dominated by GDGT-0 (93.0 ±
556 12.5%, n = 22) with low proportions of GDGT-2 (2.6 ± 9.5, n = 20) suggesting anoxic
557 conditions in Searles Lake and likely a shallower lake. Whilst sedimentary production of
558 both GDGT-0 and GDGT-2 can modify the original water column isoGDGT distribution
559 as sediments become anoxic (Blaga et al., 2009; Damsté et al., 2012), the observed
560 GDGT abundance distributions most likely denote water column anoxia.

561 This combination of biomarkers has been previously used as a diagnostic for Pleistocene
562 pluvials in the adjacent SLAPP-SRLS17 core location (Peaple et al., 2022). Similar to the
563 200-ka reconstruction, we found crenarchaeol to be at vanishingly low abundance in the
564 late Pliocene being undetectable in many samples with just 3 samples having cren as
565 more than 1% of the ΣisoGDGTs (0.5 ± 1.1%, n = 29; **Figure 4**), and GDGT-0 was high,
566 thus Searles Lake was likely mostly anoxic and stratified. In one notable event in that
567 study of the last 200 ka, cren relative abundance peaked at 16% of ΣisoGDGTs and
568 GDGT-0 was low at Termination 2 at the end of MIS 6, which was interpreted as a
569 vigorously overturning deep lake phase (Peaple et al., 2022). That interpretation is
570 supported by geomorphic evidence for spillover into downstream Panamint Valley (Jayko
571 et al., 2008). This suggests that the Termination 2 pluvial was wetter than the MIS M2
572 pluvial. One caveat about the late Pliocene and late Pleistocene comparison is that
573 microbial communities may have changed over the intervening 3 Ma and there is some

574 evidence for this. Alkalinity increased in the basin following hydrothermal activity in the
575 vicinity of the Long Valley volcanic center (Lowenstein et al., 2016) and this was
576 associated with a change in the microbial community at Searles Lake as evidenced by
577 carotenoids before and after 1.4 Ma (Winters et al., 2013).

578 5.2. Mojave pluvial associated with MIS M2 glaciation

579 The evidence for a deep lake in Searles Valley associated with the MIS M2 glacial was
580 first described and dated by Liddicoat et al., (1980). Here we updated the timing of the
581 paleomagnetic datums (**Figure 2**) and sampled the lacustrine phase to refine
582 interpretations with new biomarker evidence. We find that older sediments (3.373–3.268
583 Ma) associated with the MIS M2 glacial (3.312–3.264 Ma) capture relatively cool
584 conditions (**Figure 5e**), and relatively fresh lake waters as detected by semi-quantitative,
585 independent bacterial and archaeal indicators (**Figure 5f, g**), compared to the relative
586 warmth (mean 25 ºC) and salinity rise of the subsequent mPWP (**Table 1**). There are
587 significant differences ($p<0.05$) for temperature and salinity between periods 3.370–3.264
588 Ma and 3.264–2.950 Ma which broadly align with the high latitude MIS M2 cooling
589 (cooling includes the precursor cooling of MG 4 and 2, **Figure 5b**, as identified by
590 changepoint analysis here) and extended mPWP warm periods respectively.

591 **Table 1.** Summary of the key findings

Name	**Age (Ma)**	**T (ºC)**	**Salinity**	**P-E**	**δD_{precip} (‰)**	**$\delta^{13}C$ (‰)**
MIS M2-pluvial	3.370-3.264	21±3	Low	Much wetter than modern	Unchanged	Unchanged
Extended mPWP	3.264-2.950	25±3	Moderate	Slightly wetter than modern	Unchanged	Unchanged

592 Corroboration of pluvial conditions associated with the extended MIS M2 glacial cooling
593 comes from regional comparison. The onset of lacustrine deposition at 3.4 Ma at Searles

Lake, corresponds to a perennial lake in nearby basin Death Valley (**Figure 5a**), together indicating a considerable P-E increase (Knott et al., 2018). Searles Lake records a climate (MAF mean = 21 ± 3 ºC, n = 2) similar to or slightly cooler than the modern, implying similar potential evaporation. Similar potential evaporation implies much more precipitation relative to the today was a necessary condition for the lake to fill. The fresh, deep lake represents robust evidence for cooler and wetter conditions in southwestern North America associated with the extended cooling including the late Pliocene MIS M2 glaciation, that we refer to as the "M2 pluvial", compared to drier conditions during the mid-Pliocene warmth.

5.2.1. Understanding climate and drivers of the M2 pluvial

A limitation with understanding the climate response to the MIS M2 glacial is the sparse terrestrial evidence available to date. Additional terrestrial reconstruction efforts would ideally add evidence in future, however Pliocene lacustrine sedimentary accumulations persist only in rare basins on land. Arguably, the best terrestrial archive of this time is Lake El'gygytgyn (Northeastern Russia). There, they observe a 10 ºC cooling from peak mid-Pliocene warmth to near-Holocene temperatures from 3.39 to 2.64 Ma (**Figure 5c**) inferred from pollen evidence for a shift from boreal forest to tundra (Brigham-Grette et al., 2013). That cooling in Siberia is detected by change-point analysis here (**Figure 5b**) coincident with a cooling detected in marine benthic $\delta^{18}O$ into MIS MG4 about 0.1 Ma prior to the MIS M2 glaciation (Westerhold et al., 2020).

Marine sedimentary records spanning the Pliocene are more readily available, and nearby to the Lake El'gygytgyn record, alkenones capture a 6 ºC cooling of SSTs from the Gulf of Alaska (**Figure 5d**) with the cooling also beginning at 3.4 Ma and reaching a

617 minimum during MIS M2. The absence of ice-rafted debris, however, indicates that the
618 Cordilleran ice sheet did not reach all the way to the coast (Sánchez-Montes et al., 2020).
619 The cooling is most pronounced in high latitudes, closer to the locus of terrestrial
620 glaciation, but the California Current propagates the signal southward to Site 1012
621 (32.2ºN, offshore the US-Mexico border) with a 4 ºC cooling recorded by alkenones
622 (Brierley et al., 2009). The magnitude of cooling along the coastal ocean is consistent
623 with terrestrial cooling of 4 ºC at Searles Lake (35.7ºN) – the cooling here is relative to
624 the later mPWP, as our record begins in the cool interval.

625 Globally, the MIS M2 glacial from 3.312–3.264 Ma was accompanied by a $\delta^{18}O$ increase
626 of 1.1‰ according to the latest estimates (Westerhold et al., 2020; **Figure 5b**) revised
627 upwards from the initial evidence of 0.4‰ (Shackleton & Opdyke, 1977) and 0.5‰
628 (Lisiecki & Raymo, 2005). Estimates of a 20–60 m sea level drop relative to today were
629 associated with the smaller $\delta^{18}O$ shifts, whereas lower sea levels are likely associated
630 with the 1.1‰ increase. The main uncertainties on these foraminiferal estimates of glacial
631 magnitude arise from diagenesis concerns (Raymo et al., 2018), although foraminiferal
632 preservation improved in samples from MIS M2 (De La Vega et al., 2020).

633 The MIS M2 glacial cooling was accompanied by a 100 ppmv decrease in atmospheric
634 carbon dioxide similar to that of late Pleistocene glacials, with evidence from $\delta^{11}B$ of
635 foraminifera indicating a drop from 400 ppmv to 300 ppmv (De La Vega et al., 2020).
636 The high-resolution record finds that the drop in pCO_2 lagged the orbital and $\delta^{18}O$
637 oscillation, thus another mechanism for the initiation of the glacial event is required. That
638 trigger may have been the re-opening of the shallow Central American Seaway altering
639 circulation between the Pacific and Atlantic and thus the heat flux to the high latitude

Atlantic Ocean (De Schepper et al., 2014; Tan et al., 2017).

Model experiments to test sensitivity during the MIS M2 glaciation find only the large ice sheet scenario produces a measurable change in precipitation and drying in southwestern North America (Dolan et al., 2015). The modelled drying is at odds with the evidence for a pluvial presented here. Given that late Pleistocene glacial conditions are associated with pluvials in the southwest, we posit that similar mechanisms could have operated in the Pliocene (Fu, 2023; Lofverstrom, 2020; McGee et al., 2018a). Further elucidation of the climate dynamics will have to await additional MIS M2 simulations that succeed in representing the glacial-pluvial conditions.

5.3. Drying and warming into the mPWP

After the MIS M2 glacial, we find evidence for warming and drying at the start of an extended warm phase, the mPWP. The warm period spanning 3.264–3.025 Ma (MIS M1 through MIS G21) is the focus of PRISM and a series of PlioMIP model and proxy intercomparisons. We report new terrestrial brGDGT-based paleothermometry evidence that Searles Valley was 4 ºC warmer during the mPWP than during the M2 event. We find br- and isoGDGT evidence for an increase in salinity and increasing proportion of GDGT-0 suggesting a saltier, shallower and more stratified (anoxic) lake. Although the mPWP was drier than the cool M2 glacial pluvial, the warm period likely received more precipitation than modern, given the presence of a perennial lake. High f(GDGT-0) indicates that the lake was largely anoxic and was thus not well mixed, likely a shallow, salty lake with no outflow.

Globally, annual mean temperatures were around 3.5 ºC higher in the mPWP warm period than today (Burke et al., 2018; Dowsett & Caballero Gill, 2010; Haywood et al.,

663 2020; Ravelo et al., 2004). Consistent with global warmth during the mPWP, we find
664 mean reconstructed mPWP MAF temperatures at Searles Lake (24 ± 3 ºC, n = 5).
665 Although terrestrial quantitative temperature estimates remain rare, supporting evidence
666 for warming comes from diatom assemblage studies from Tule Lake, Northern California
667 (**Figure 1**), that found *Aulacoseira solida* abundances increased coincident with the
668 mPWP before an increase in *Fragilaria* spp. denoting cooling likely associated with the
669 intensification of Pleistonce Northern Hemisphere glaciation (Thompson, 1991).
670 A local warming of 4 ºC from M2 into the mPWP would imply a higher evaporation rate
671 than currently exists in Searles Valley. Today Searles Valley lowland receives 100
672 mm/year precipitation, with ~2000 mm/year potential evaporation. During pluvials with
673 inflowing Owens River, the catchment included the eastern Sierra Nevada which has
674 modern precipitation of around 400 mm/year (Lake Sabrina, Western Regional Climate
675 Center., 2022). Menemenlis et al. (2022) performed calculations for the southern Great
676 Basin region; in their wettest scenario they estimate that sustaining a 18.6% lake
677 coverage would require 1.0 mm/day (2.5x) more rainfall across the broad region, given a
678 similar-to-modern temperature regime. As the spatial heterogeneity of a mountain
679 catchment is not well represented by such a calculation, and as the large regional areas of
680 lakes in the northern reaches of their study area are beyond the scope of this study, we
681 cannot directly relate their calculations to Searles Lake. We do not attempt lake water
682 balance calculations for Searles Lake as the volume of the Pliocene basin is unclear, but a
683 doubling of modern precipitation to fill a deep lake seems plausible.

684 Referring again to the southern Great Basin calculations for the dry and intermediate
685 scenario of Menemenlis et al. (2022), with 1.6 and 3.6% lake coverage, then a saline lake

686 could imply up to 0.4 mm/day (1.2x) more precipitation over the broad region compared
687 to today. Downscaling quantitative reconstructions of basin water balance and climate for
688 Searles Lake must await refinement of the basin size as well as a realistic treatment of
689 precipitation change across the topography of the catchment in climate models. However,
690 the Searles Lake proxy data are consistent with wetter-than-modern conditions during the
691 mPWP to produce the intermittent/saline lake, under elevated temperatures, however
692 conditions were drier than in the M2 pluvial.

693 5.3.1. Carbon isotopic reconstructions

694 $\delta^{13}C$ values for the *n*-alkanoic acids indicate a trend of ^{13}C-depletion across chain lengths
695 from C_{24} to C_{30}. The isotopic spread likely relates to shifting proportions of various
696 producers of long-chain *n*-alkanoic acids, with measured variations among terrestrial
697 plants in the region, as well as possible macrophyte inputs (Peaple et al., 2021). We show
698 the C_{28} *n*-alkanoic acids (-31.6 to -27.0‰) and C_{30} *n*-alkanoic acids -34.0 to -28.4‰ (-
699 30.7 ± 1.4‰, n = 28; **Figure 3g**), with C_{30} being most ^{13}C-depleted and most likely
700 indicative of terrestrial plants.

701 These carbon isotopic values are consistent with the trees and shrubs sampled in the
702 modern catchment, with *n*-alkanoic acid production likely dominated by the coniferous
703 taxa, with $\delta^{13}C$ values of -29.7‰ for *Juniperus occidentalis*, -24.7‰ for *Abies concolor,*
704 and -25‰ for *Pinus jeffreyi* (Peaple et al., 2022). Coniferous taxa tend to produce plant
705 wax with a high proportion of *n*-alkanoic acid to *n*-alkanes (Diefendorf et al., 2011), as
706 also measured in local trees (Peaple et al., 2021) and fluvial runoff (Feakins et al., 2019).
707 Conifers expanded their lowland range in cooler, wetter times of the Pleistocene based on
708 macro- and microfossils (Wolfenden, 2003; Holmgren et al., 2010; Koehler et al., 2005;

709 Peaple et al., 2022). However, the $\delta^{13}C$ values of the *n*-alkanoic acids were not
710 significantly different between the last glacial maximum and interglacial of the late
711 Pleistocene. While conifers may have also expanded into the lowlands during the M2
712 pluvial, the $\delta^{13}C$ values of the *n*-alkanoic acids are not significantly different from that of
713 the mPWP, with both high and low values within each interval. Overall, the $\delta^{13}C$ values
714 of the *n*-alkanoic acids are lower in this late Pliocene record than the late Pleistocene
715 (Peaple et al., 2022).

716 The *n*-alkanes and pollen together provided evidence for varying proportions of
717 C_4 phreatophytic shrubs (including Atriplex) during the Pleistocene (Peaple et al., 2022),
718 however *n*-alkanes and pollen are not preserved in these Pliocene sediments rendering
719 vegetation largely unknown for the Pliocene in this basin. We note the M2 glacial drop in
720 pCO_2 was from 400 to 300 ppmv (De La Vega et al., 2020), thus atmospheric conditions
721 would have been less favorable for C_4 than during the late Pleistocene glacials, which
722 were another 100 ppmv lower at 180 ppmv (Petit et al., 1999).

723 Coeval with warming and drying into the mPWP, we find an increase in *n*-alkanoic acid
724 $\delta^{13}C$ (from -34 to -28‰) across 3.4–2.9 Ma. We note a positive correlation between lake
725 salinity, as measured by ACE and $\delta^{13}C_{wax}$ (C_{30} r = 0.51, p = 0.05 and C_{28} r = 0.45, p =
726 0.15) accounting for serial correlation (Ebisuzaki, 1997). The range of values are
727 consistent with open C_3 vegetation in the region today (Peaple et al., 2022), and so the
728 shift may indicate range changes among those species: perhaps Pinus expansion into
729 higher elevations after the M2 glacial, and a reduction in Juniper in the lowlands due to
730 drying. In addition, the $\delta^{13}C$ increase may indicate an increase in moisture stress among
731 C_3 plants (Diefendorf et al., 2010). Alternatively, the trend could indicate C_4 plant

732 contributions. Similar carbon isotope enrichment trends in the late Pliocene have been
733 reported from soil carbonates, from Camp Rice, New Mexico (Mack et al., 1994), and
734 from St David, Arizona, where the trend represents C_4 grassland expansion reflecting
735 warming and summer (North American Monsoon; NAM) rainfall (Y. Wang et al., 1993).
736 Recent proxy and modeling work suggests that the NAM may have expanded into
737 southern California during the mPWP (Fu et al., 2022; Bhattacharya et al., 2022), which
738 could lead to C_4 expansion. However, the vegetation of the Mojave lowlands and Sierra
739 Nevada watershed remains an open question until in situ Pliocene paleobotanical macro
740 or microfossil clues are found.

741 5.4. Precipitation isotope reconstructions

742 The δD_{precip} reconstruction for Searles Lake in the late Pliocene does not show any
743 change between the M2 glacial pluvial and the mPWP, nor from the Pleistocene. δD_{precip}
744 reconstructions based on *n*-alkanoic acids for 3.373 to 2.706 Ma from KM-3 (-89 ± 5‰,
745 n = 25, this study) are 10‰ more D-depleted than reconstructions from SLAPP-SRLS17
746 spanning 200 to 4 ka (-77 ± 18‰, n = 112; Peaple et al., 2022). These reconstructions are
747 the same within uncertainties given the different sample size, temporal variability and
748 sampling resolution. Each of these Searles Lake *n*-alkanoic acid δD_{precip} reconstructions
749 fall within the seasonal means of the modern climatology. In the late Pleistocene δD
750 reconstruction, the *n*-alkanes were the preferred compound class, reflecting the expected
751 pattern of glacial D-depletion and interglacial D-enrichment seen in the *n*-alkanes and in
752 other regional reconstructions (Peaple et al., 2022). Whereas the *n*-alkanoic acid evidence
753 was deemed less useful through comparisons in the Pleistocene (Peaple et al., 2022), with
754 downcore variability perhaps confounded by changes in conifer elevation and

755 macrophyte inputs (Peaple et al., 2021), the Pliocene plant wax reconstructions therefore
756 must remain tentative.

757 Independent evidence for δD_{precip} values during the MIS M2 glaciation, has previously
758 been reported from the Owens River watershed (Mulch et al., 2008), part of the Searles
759 Valley catchment. Using the waters of hydration extracted from the Nomlaki Tuff (ca.
760 3.30 Ma; Knott et al., 2018) sampled in Fish Lake Valley, Mulch et al. (2008) estimated
761 δD_{precip} was -144‰ when the Nomlaki Tuff was deposited. Mulch et al. (2008)
762 hypothesize that the hydration rinds of the volcanic glass shards formed within 10^3 -10^4
763 years after eruption and deposition, and thus the δD values integrate MIS M2 glacial
764 precipitation. The δD_{precip} from hydration of tephra indicates winter-precipitation
765 dominated the MIS M2 glacial adjacent to the Searles Valley catchment. The -144‰
766 value of the hydrated glass shards is more D-depleted than modern mean annual
767 precipitation, but is similar to values recorded during high precipitation winter storms in
768 the Southern Great Basin (Friedman et al., 1992, 2002).

769 Today the Searles Lake catchment receives dominantly winter orographic precipitation
770 passing over or leaking to the south of the Sierra Nevada with rare summer rain much of
771 which is lost to evaporation (Friedman et al., 2002). In the Pliocene evidence indicates
772 precipitation was also dominated by winter storms distilled over the Sierra Nevada
773 (Mulch et al., 2008) and tentatively corroborated by our plant wax *n*-alkanoic acid
774 evidence. Although regional summer monsoonal rains increased in intensity
775 (Bhattacharya et al., 2022), they likely reflected a minor contribution to the Searles Lake
776 catchment. The isotopic evidence east of the Sierra Nevada (tephra, plant wax) requires
777 only an increase in the number rather than seasonality or trajectory of storm tracks

778 delivering the P-E excess filling large lakes during the MIS M2 glacial pluvial. The M2
779 pluvial was followed by relatively drier conditions during the mPWP although still
780 requiring more rain than today to sustain a perennial lake. In the modern climate of
781 California, inter-annual variability is linked to a few extra extreme storms, with the
782 wettest 5% of days explaining 1/3 of the annual precipitation but 2/3 of the variance with
783 most of this falling on the Sierra Nevada (Dettinger, 2016). Similarly, the receipt of a few
784 more extreme storms each year, could explain a pluvial phase that filled Searles Lake,
785 lasting 150 ka around the MIS M2 glacial cooling.

786 Further south, in what is now the Anza Borrego Desert (31.4°N), 400 km south of Searles
787 and 100 km inland from the Gulf of California and Pacific Ocean, a petrified laurel-
788 willow-walnut forest of late Pliocene age required increased precipitation and incursions
789 of coastal fog (Remeika et al., 1988). However, ODP Site 1012 (**Figure 1**) marine core
790 isotopic evidence suggests summer rather than the originally proposed winter-season
791 precipitation increase (Bhattacharya et al., 2022). In that study, plant wax reconstructions
792 from marine core sites ODP Site 1012 and DSDP Site 475 (**Figure 1**) found δD_{precip}
793 values were 20‰ heavier than modern across 3.5–3 Ma, consistent with a strengthened
794 North American Monsoon (Bhattacharya et al., 2022). They linked strengthened NAM to
795 reduced subtropical to equatorial eastern Pacific SSTs in the warmer background state of
796 the late Pliocene (that study did not have the temporally resolution to detect any
797 perturbation associated with the MIS M2 glacial cooling). A strengthened NAM would
798 likely have increased summer precipitation over Searles Lake at the northwestern edge of
799 the modern NAM region (Western Regional Climate Center., 2023). Currently, the
800 Searles Catchment receives only 10% of its mean annual precipitation during the NAM

months of July, June, and August (Western Regional Climate Center., 2023) and much of this is lost to evaporation, not reaching groundwater or plants (Carroll et al., 2020). However, modeling of the NAM expansion (Fu et al., 2022 Bhattacharya et al., 2022) suggests a substantial incursion of summer rainfall is possible for the mPWP, suggesting that summer rain could have contributed to the higher Searles lake levels. In addition, if summer humidity increased substantially, summer evaporative losses would decrease and the water may have become more available to plants and groundwater recharge.

5.5. Climate dynamics during the MIS M2 glacial pluvial

Although ice sheet extent is not well constrained for the Pliocene MIS M2 glaciation globally, or for the Cordilleran Ice Sheet (Sánchez-Montes et al, 2020), the Laurentide Ice Sheet extended over Hudson Bay (Gao et al., 2012). The presence of a large LIS during the MIS M2 glaciation, would have depressed the winter storm track southward leading to an increased moisture flux to the mid-latitudes. We hypothesize that the Pliocene MIS M2 glaciation may have yielded more inland penetrating atmospheric rivers with similar dynamics to those of the modern climate (Rutz et al., 2015) due to similar topography, but with greater frequency or amount of moisture transported to explain the filled lake basins. Although we invoke similar mechanisms to the late Pleistocene glacial pluvials, the 30x longer duration of the extended M2 pluvial merits further investigation.

Prior efforts to understand the climate of late Pliocene warmth have integrated time-slabs and this may have resulted in an under-appreciation of the orbital-scale variability within the late Pliocene (Prescott et al., 2014). This has been hypothesized to be behind some of

the proxy-model disagreement (Haywood, et al., 2013). The biomarker reconstruction from Searles Lake core KM-3, provides clarification that the pluvial conditions were associated with MIS M2 glaciation (and cooling associated with the MG4 and MG2 precursors) followed by drier conditions within the mPWP (**Table 1**), although still wetter than modern conditions. We hope the new biomarker evidence can refresh interest in modelling the MIS M2 glacial (Dolan et al., 2015), to elucidate the climate dynamics that explain the pluvial conditions, reconstructed here.

6. Conclusions

Applying biomarker proxies to sediments from the KM-3 core of Searles Valley, California, we have demonstrated variable lacustrine conditions during the late Pliocene, a period previously interpreted as a continuously deep lake (Smith et al., 1983). Continuous sedimentation and a lacustrine record through the Mammoth reversal subchron make Searles Lake a valuable subtropical (35.7ºN) terrestrial archive of conditions during the MIS M2 glacial. We find that the MIS M2 glacial was locally a cool pluvial, with a deep lake from 3.4 to 3.2 Ma consistent with other interpretations (Knott et al., 2018; Liddicoat et al., 1980). Warming into the mPWP led to a saline lake that persisted for ~0.6 Ma before lake desiccation. The biomarker salinity evidence is corroborated by a positive shift in carbon isotopes of plant waxes as well as prior observations of evaporites in the lake sediments (Smith et al., 1983).

Intense pluvial conditions of the late Pliocene were confined a statistically defined cooling detected in the benthic oxygen isotope record, around the MIS M2 glaciation that interrupted warmth, much as the pluvial states of the late Pleistocene. As we reconstruct temperatures locally only slightly cooler than today during MIS M2 at Searles Lake,

evaporation would only be slightly lower and the P-E surplus to necessary to fill a deep lake must be dominated by increased rainfall (Ibarra et al., 2018). During the subsequent warmth of the mPWP, the persistence of a perennial lake implies more rainfall than present to yield a slight P-E surplus. Additional studies are needed to add spatial and temporal resolution to the nature of the climate transitions across the MIS M2 glacial and mPWP.

Acknowledgments

The biomarker study and GRA (Peaple) were supported by U.S. National Science Foundation Grant NSF-EAR-1903665 to S.F., GDGT analyses were supported by the Packard Fellowship for Science and Engineering to J.T. and NSF-OCE-1903171 to J.T. T.B. was supported by NSF-OCE-1903148. JRK was supported by National Science Foundation Integrated Earth Sciences grant EAR-1516593. Sample material used in this project was provided by USGS Core Research Center. We thank Patrick Murphy for his assistance in preparing and measuring GDGTs. We thank colleagues for helpful discussions at Pliocene workshops including Peter Molnar, Erin McClymont, Bette Otto Bleisner and Alan Haywood. We thank Dan Ibarra, Ran Feng and Joe Liddicoat for reading earlier versions of the manuscript.

Open Research

Data files are archived at the NOAA paleoclimatology database and will be made publicly available prior to acceptance (Peaple et al., 2023). Data is temporarily available to reviewers as supplementary information.

References

Almazroui, M., Islam, M. N., Saeed, F., Saeed, S., Ismail, M., Ehsan, M. A., et al. (2021). Projected Changes in Temperature and Precipitation Over the United States, Central America, and the Caribbean in CMIP6 GCMs. *Earth Systems and Environment 2021 5:1*, *5*(1), 1–24. https://doi.org/10.1007/S41748-021-00199-5

Bacon, S. N., Jayko, A. S., Owen, L. A., Lindvall, S. C., Rhodes, E. J., Schumer, R. A., & Decker, D. L. (2020). A 50,000-year record of lake-level variations and overflow from Owens Lake, eastern California, USA. *Quaternary Science Reviews*, *238*, 106312. https://doi.org/10.1016/j.quascirev.2020.106312

Baxter, A. J., van Bree, L. G. J., Peterse, F., Hopmans, E. C., Villanueva, L., Verschuren, D., & Sinninghe Damsté, J. S. (2021). Seasonal and multi-annual variation in the abundance of isoprenoid GDGT membrane lipids and their producers in the water column of a meromictic equatorial crater lake (Lake Chala, East Africa). *Quaternary Science Reviews*, *273*, 107263. https://doi.org/10.1016/J.QUASCIREV.2021.107263

Besseling, M. A., Hopmans, E. C., Boschman, R. C., Sinninghe Damsté, J. S., & Villanueva, L. (2018). Benthic archaea as potential sources of tetraether membrane lipids in sediments across an oxygen minimum zone. *Biogeosciences*, *15*(13), 4047–4064.

Bhattacharya, T., Tierney, J. E., Addison, J. A., & Murray, J. W. (2018). Ice-sheet modulation of deglacial North American monsoon intensification. *Nature Geoscience*, 1. https://doi.org/10.1038/s41561-018-0220-7

Bhattacharya, T., Feng, R., Tierney, J. E., Rubbelke, C., Burls, N., Knapp, S., & Fu, M. (2022). Expansion and Intensification of the North American Monsoon During the Pliocene. *AGU Advances*, *3*(6). https://doi.org/10.1029/2022av000757

Blaauw, M., & Christeny, J. A. (2011). Flexible paleoclimate age-depth models using an autoregressive gamma process. *Bayesian Analysis*, *6*(3), 457–474. https://doi.org/10.1214/11-BA618

Blackwelder, E. (1933). Lake Manly: An Extinct Lake of Death Valley. *Geographical Review*, *23*(3), 464. https://doi.org/10.2307/209632

Blaga, C. I., Reichart, G.-J., Heiri, O., & Sinninghe Damsté, J. S. (2009). Tetraether membrane lipid distributions in water-column particulate matter and sediments: a study of 47 European lakes along a north–south transect. *Journal of Paleolimnology*, *41*(3), 523–540.

Brigham-Grette, J., Melles, M., Minyuk, P., Andreev, A., Tarasov, P., DeConto, R., et al. (2013). Pliocene warmth, polar amplification, and stepped Pleistocene cooling recorded in NE Arctic Russia. *Science*, *340*(6139), 1421–1427.

Brittingham, A., Hren, M. T., & Hartman, G. (2017). Microbial alteration of the hydrogen and carbon isotopic composition of n-alkanes in sediments. *Organic Geochemistry*, *107*, 1–8. https://doi.org/10.1016/j.orggeochem.2017.01.010

Burke, K. D., Williams, J. W., Chandler, M. A., Haywood, A. M., Lunt, D. J., & Otto-Bliesner, B. L. (2018). Pliocene and Eocene provide best analogs for near-future climates. *Proceedings of the National Academy of Sciences*, *115*(52), 13288–13293.

Carroll, R. W., Deems, J. S., Niswonger, R., Schumer, R., & Williams, K. H. (2019). The importance of interflow to groundwater recharge in a snowmelt-dominated headwater basin. *Geophysical Research Letters*, *46*(11), 5899-5908.

Carroll, R. W., Gochis, D., & Williams, K. H. (2020). Efficiency of the summer monsoon in generating streamflow within a snow-dominated headwater basin of the Colorado River. *Geophysical Research Letters*, *47*(23), e2020GL090856.

Channell, J. E. T., Singer, B. S., & Jicha, B. R. (2020). Timing of Quaternary geomagnetic reversals and excursions in volcanic and sedimentary archives. *Quaternary Science Reviews*, *228*, 106114. https://doi.org/10.1016/J.QUASCIREV.2019.106114

Chiang, J. C. H., Lee, S. Y., Putnam, A. E., & Wang, X. (2014). South Pacific Split Jet, ITCZ shifts, and atmospheric North–South linkages during abrupt climate changes of the last glacial period. *Earth and Planetary Science Letters*, *406*, 233–246. https://doi.org/10.1016/J.EPSL.2014.09.012

Choi, J., Lu, J., Son, S. W., Frierson, D. M. W., & Yoon, J. H. (2016). Uncertainty in future projections of the North Pacific subtropical high and its implication for California winter precipitation change. *Journal of Geophysical Research: Atmospheres*, *121*(2), 795–806. https://doi.org/10.1002/2015JD023858

Curry, R. R. (1966). Glaciation about 3,000,000 years ago in the Sierra Nevada. *Science*, *154*(3750), 770–771.

Damsté, J. S. S., Weber, Y., Zopfi, J., Lehmann, M. F., & Niemann, H. (2022). Distributions and sources of isoprenoidal GDGTs in Lake Lugano and other central European (peri-) alpine lakes: Lessons for their use as paleotemperature proxies. *Quaternary Science Reviews*, *277*, 107352.

De Schepper, S., Groeneveld, J., Naafs, B. D. A., Van Renterghem, C., Hennissen, J., Head, M. J., et al. (2013). Northern hemisphere glaciation during the globally warm early late Pliocene. *PloS One*, *8*(12), e81508.

Diefendorf, A. F., Freeman, K. H., Wing, S. L., & Graham, H. V. (2011). Production of n-alkyl lipids in living plants and implications for the geologic past. *Geochimica et Cosmochimica Acta*, *75*(23), 7472–7485.

939 Dolan, A. M., Haywood, A. M., Hunter, S. J., Tindall, J. C., Dowsett, H. J., Hill, D. J., &
940 Pickering, S. J. (2015). Modelling the enigmatic Late Pliocene Glacial Event —
941 Marine Isotope Stage M2. *Global and Planetary Change*, *128*, 47–60.
942 https://doi.org/10.1016/J.GLOPLACHA.2015.02.001

943 Dowsett, H. J., & Caballero Gill, R. P. (2010). Pliocene climate. *Stratigraphy*, *7*(2–3),
944 106–110.

945 European Space Agency, Sinergise (2021). Copernicus Global Digital Elevation Model.
946 Distributed by OpenTopography. https://doi.org/10.5069/G9028PQB. Accessed:
947 2023-05-02

948 Farquhar, G., & Richards, R. (1984). Isotopic composition of plant carbon correlates with
949 water-use efficiency of wheat genotypes. *Australian Journal of Plant Physiology*,
950 *11*(6), 539. https://doi.org/10.1071/PP9840539

951 Feakins, S. J., & Sessions, A. L. (2010). Controls on the D/H ratios of plant leaf waxes in
952 an arid ecosystem. *Geochimica et Cosmochimica Acta*, *74*(7), 2128–2141.
953 https://doi.org/10.1016/J.GCA.2010.01.016

954 Feakins, S. J., Kirby, M. E., Cheetham, M. I., Ibarra, Y., & Zimmerman, S. R. H. (2014).
955 Fluctuation in leaf wax D/H ratio from a southern California lake records significant
956 variability in isotopes in precipitation during the late Holocene. *Organic*
957 *Geochemistry*, *66*, 48–59. https://doi.org/10.1016/J.ORGGEOCHEM.2013.10.015

958 Feakins, S. J., Wu, M. S., Ponton, C., & Tierney, J. E. (2019). Biomarkers reveal abrupt
959 switches in hydroclimate during the last glacial in southern California. *Earth and*
960 *Planetary Science Letters*, *515*, 164–172. https://doi.org/10.1016/j.epsl.2019.03.024

961 Friedman, I., Smith, G. I., Gleason, J. D., Warden, A., & Harris, J. M. (1992). Stable
962 isotope composition of waters in southeastern California 1. Modern precipitation.
963 *Journal of Geophysical Research*, *97*(D5), 5795. https://doi.org/10.1029/92JD00184

964 Friedman, I., Harris, J. M., Smith, G. I., & Johnson, C. A. (2002). Stable isotope
965 composition of waters in the Great Basin, United States 1. Air-mass trajectories.
966 *Journal of Geophysical Research: Atmospheres*, *107*(D19), ACL 14-1.
967 https://doi.org/10.1029/2001JD000565

968 Fu, M., Cane, M. A., Molnar, P., & Tziperman, E. (2022). Warmer Pliocene upwelling
969 site SST leads to wetter subtropical coastal areas: A positive feedback on
970 SST. *Paleoceanography and Paleoclimatology*, *37*(2), e2021PA004357

971 Gagnon, C., Butler, K., Gaviria, E., Terrazas, A., Gao, A., Bhattacharya, T., et al. (2022).
972 *Paleoclimate controls on lithium enrichment in Great Basin Pliocene-Pleistocene*
973 *lacustrine clays*. https://doi.org/10.31223/X54D15

974 Gao, C., McAndrews, J. H., Wang, X., Menzies, J., Turton, C. L., Wood, B. D., et al.
975 (2012). Glaciation of North America in the James Bay Lowland, Canada, 3.5 Ma.
976 *Geology*, *40*(11), 975–978. https://doi.org/10.1130/G33092.1

977 Hammond, W. C., Blewitt, G., Li, Z., Plag, H. P., & Kreemer, C. (2012). Contemporary
978 uplift of the Sierra Nevada, western United States, from GPS and inSAR
979 measurements. *Geology*, *40*(7), 667–670. https://doi.org/10.1130/G32968.1

980 Hay, R. L., & Guldman, S. G. (1987). Diagenetic alteration of silicic ash in Searles Lake,
981 California. *Clays and Clay Minerals*, *35*, 449–457.

982 Hay, R. L., Guldman, S. G., Matthews, J. C., Lander, R. H., Duffin, M. E., & Kyser, T.
983 K. (1991). Clay mineral diagenesis in core KM-3 of Searles Lake, California. *Clays*
984 *and Clay Minerals*, *39*(1), 84–96. https://doi.org/10.1346/CCMN.1991.0390111

985 Haywood, A. M., Dolan, A. M., Pickering, S. J., Dowsett, H. J., Mcclymont, E. L.,
986 Prescott, C. L., et al. (2013). On the identification of a Pliocene time slice for data-
987 model comparison. *Philosophical Transactions of the Royal Society A:*
988 *Mathematical, Physical and Engineering Sciences*, *371*(2001).
989 https://doi.org/10.1098/rsta.2012.0515

990 Haywood, A. M., Dowsett, H. J., & Dolan, A. M. (2016). Integrating geological archives
991 and climate models for the mid-Pliocene warm period. *Nature Communications*
992 *2016 7:1*, *7*(1), 1–14. https://doi.org/10.1038/ncomms10646

993 Haywood, A. M., Tindall, J. C., Dowsett, H. J., Dolan, A. M., Foley, K. M., Hunter, S. J.,
994 et al. (2020). The Pliocene Model Intercomparison Project Phase 2: large-scale
995 climate features and climate sensitivity. *Climate of the Past*, *16*(6), 2095–2123.

996 Heusser, L. E. (1981). Pollen Analysis of Selected Samples from Deep Sea Drilling
997 Project Leg 63 vol. 28. Initial Report of DSDP; 1981. p. 559–63.
998 https://doi.org/10.2973/dsdp.proc.63.115.1981

999 Hildreth, W., Fierstein, J., & Calvert, A. T. (2018). McGee Till—oldest glacial deposit in
1000 the Sierra Nevada, California— and Quaternary evolution of the rangefront
1001 escarpment. *Quaternary Science Reviews*, *198*, 242–265.
1002 https://doi.org/10.1016/J.QUASCIREV.2018.08.008

1003 Hopmans, E. C., Schouten, S., & Sinninghe Damsté, J. S. (2016). The effect of improved
1004 chromatography on GDGT-based palaeoproxies. *Organic Geochemistry*, *93*, 1–6.
1005 https://doi.org/10.1016/j.orggeochem.2015.12.006

1006 Hren, M. T., Pagani, M., Erwin, D. M., & Brandon, M. (2010). Biomarker reconstruction
1007 of the early Eocene paleotopography and paleoclimate of the northern Sierra
1008 Nevada. *Geology*, *38*(1), 7–10. https://doi.org/10.1130/G30215.1

1009 Huguet, C., Hopmans, E. C., Febo-Ayala, W., Thompson, D. H., Sinninghe Damsté, J. S.,
1010 & Schouten, S. (2006). An improved method to determine the absolute abundance of

glycerol dibiphytanyl glycerol tetraether lipids. *Organic Geochemistry*, *37*(9), 1036–1041. https://doi.org/10.1016/J.ORGGEOCHEM.2006.05.008

Ibarra, D. E., Oster, J. L., Winnick, M. J., Caves Rugenstein, J. K., Byrne, M. P., & Chamberlain, C. P. (2018). Warm and cold wet states in the western United States during the Pliocene–Pleistocene. *Geology*, *46*(4), 355–358. https://doi.org/10.1130/G39962.1

Jacobel, A. W., McManus, J. F., Anderson, R. F., & Winckler, G. (2016). Large deglacial shifts of the Pacific intertropical convergence zone. *Nature Communications*, *7*(1), 1–7.

Jayko, A. S., Forester, R. M., Kaufman, D. S., Phillips, F. M., Yount, J. C., McGeehin, J., & Mahan, S. A. (2008). Late Pleistocene lakes and wetlands, Panamint Valley, Inyo County, California. In *Special Paper of the Geological Society of America* (Vol. 439, pp. 151–184). https://doi.org/10.1130/2008.2439(07)

Jayko, A. S., Bacon, S. N., Reheis, M. C., Hershler, R., & Miller, D. M. (2008). Late Quaternary, MIS 6-8 shoreline features of pluvial Owens Lake, Owens Valley, eastern California. *SPECIAL PAPERS-GEOLOGICAL SOCIETY OF AMERICA*, *439*, 185.

Keisling, B. A., Castañeda, I. S., & Brigham-Grette, J. (2017). Hydrological and temperature change in Arctic Siberia during the intensification of Northern Hemisphere Glaciation. *Earth and Planetary Science Letters*, *457*, 136–148. https://doi.org/10.1016/J.EPSL.2016.09.058

Knott, J. R., Machette, M. N., Klinger, R. E., Sarna-Wojcicki, A. M., Liddicoat, J. C., Tinsley, J. C., et al. (2008). Reconstructing late Pliocene to middle Pleistocene Death Valley lakes and river systems as a test of pupfish (Cyprinodontidae) dispersal hypotheses. In *Special Paper of the Geological Society of America* (Vol. 439, pp. 1–26). Geological Society of America. https://doi.org/10.1130/2008.2439(01)

Knott, J. R., Machette, M. N., Wan, E., Klinger, R. E., Liddicoat, J. C., Sarna-Wojcicki, A. M., et al. (2018). Late Neogene–Quaternary tephrochronology, stratigraphy, and paleoclimate of Death Valley, California, USA. *GSA Bulletin*, *130*(7–8), 1231–1255. https://doi.org/10.1130/B31690.1

Knott, J. R., Wan, E., Deino, A. L., Casteel, M., Reheis, M. C., Phillips, F. M., et al. (2019). Lake Andrei: A pliocene pluvial lake in Eureka Valley, eastern California. *From Saline to Freshwater: The Diversity of Western Lakes in Space and Time, S. Starratt and MR Rosen, Eds*, *536*, 125–142.

Knott, J. R., Liddicoat, J. C., Coe, R. S., & Negrini, R. M. (2021). Radiocarbon and paleomagnetic chronology of the Searles Lake Formation, San Bernardino County,

California, USA. *From Saline to Freshwater: The Diversity of Western Lakes in Space and Time*, 81–95. https://doi.org/10.1130/2018.2536(06)

De La Vega, E., Chalk, T. B., Wilson, P. A., Bysani, R. P., & Foster, G. L. (2020). Atmospheric CO2 during the Mid-Piacenzian Warm Period and the M2 glaciation. *Scientific Reports*, *10*(1), 1–8.

Lachniet, M. S., Denniston, R. F., Asmerom, Y., & Polyak, V. J. (2014). Orbital control of western North America atmospheric circulation and climate over two glacial cycles. *Nature Communications*, *5*(1), 3805. https://doi.org/10.1038/ncomms4805

Liddicoat, J. C., Opdyke, N. D., & Smith, G. I. (1980). Palaeomagnetic polarity in a 930-m core from Searles Valley, California. *Nature*, *286*(5768), 22–25. https://doi.org/10.1038/286022a0

Lindberg, K. R., Daniels, W. C., Castañeda, I. S., & Brigham-Grette, J. (2022). Biomarker proxy records of Arctic climate change during the Mid-Pleistocene transition from Lake El'gygytgyn (Far East Russia). *Climate of the Past*, *18*(3), 559–577.

Lisiecki, L. E., & Raymo, M. E. (2005). A Pliocene-Pleistocene stack of 57 globally distributed benthic δ 18O records. *Paleoceanography*, *20*(1), 1–17. https://doi.org/10.1029/2004PA001071

Lofverstrom, M. (2020). A dynamic link between high-intensity precipitation events in southwestern North America and Europe at the Last Glacial Maximum. *Earth and Planetary Science Letters*, *534*, 116081.

Lora, J. M., Mitchell, J. L., Risi, C., & Tripati, A. E. (2017). North Pacific atmospheric rivers and their influence on western North America at the Last Glacial Maximum. *Geophysical Research Letters*, *44*(2), 1051-105.

Lowenstein, T. K., Dolginko, L. A. C., & García-Veigas, J. (2016). Influence of magmatic-hydrothermal activity on brine evolution in closed basins: Searles Lake, California. *Bulletin*, *128*(9–10), 1555–1568.

Mack, G. H., Giordano, T. H., Cole, D. R., James, W. C., & Salyards, S. L. (1994). Stable oxygen and carbon isotopes of pedogenic carbonate as indicators of Plio-Pleistocene paleoclimate in the southern Rio Grande Rift, south-central New Mexico. *American Journal of Science;(United States)*, *294*(5).

Martínez-Botí, M. A., Foster, G. L., Chalk, T. B., Rohling, E. J., Sexton, P. F., Lunt, D. J., et al. (2015). Plio-Pleistocene climate sensitivity evaluated using high-resolution CO2 records. *Nature*, *518*(7537), 49–54. https://doi.org/10.1038/nature14145

Martínez-Sosa, P., Tierney, J. E., Stefanescu, I. C., Dearing Crampton-Flood, E., Shuman, B. N., & Routson, C. (2021). A global Bayesian temperature calibration for

lacustrine brGDGTs. *Geochimica et Cosmochimica Acta*, *305*, 87–105. https://doi.org/10.1016/J.GCA.2021.04.038

McGee, D., Moreno-Chamarro, E., Marshall, J., & Galbraith, E. D. (2018a). Western U.S. lake expansions during Heinrich stadials linked to Pacific Hadley circulation. *Science Advances*, *4*(11). https://doi.org/10.1126/SCIADV.AAV0118/SUPPL_FILE/AAV0118_SM.PDF

McGee, D., Moreno-Chamarro, E., Marshall, J., & Galbraith, E. D. (2018b). Western U.S. lake expansions during Heinrich stadials linked to Pacific Hadley circulation. *Science Advances*, *4*(11), eaav0118. https://doi.org/10.1126/sciadv.aav0118

McPhillips, D., & Brandon, M. T. (2010). Using tracer thermochronology to measure modern relief change in the Sierra Nevada, California. *Earth and Planetary Science Letters*, *296*(3–4), 373–383. https://doi.org/10.1016/j.epsl.2010.05.022

Menemenlis, S., White, S. M., Ibarra, D. E., & Lora, J. M. (2022). A proxy-model comparison for mid-Pliocene warm period hydroclimate in the Southwestern US. *Earth and Planetary Science Letters*, *596*, 117803.

Mix, H. T., Ibarra, D. E., Mulch, A., Graham, S. A., & Page Chamberlain, C. (2016). A hot and high Eocene Sierra Nevada. *Bulletin of the Geological Society of America*, *128*(3–4), 531–542. https://doi.org/10.1130/B31294.1

Mix, H. T., Caves Rugenstein, J. K., Reilly, S. P., Ritch, A. J., Winnick, M. J., Kukla, T., & Chamberlain, C. P. (2019). Atmospheric flow deflection in the late Cenozoic Sierra Nevada. *Earth and Planetary Science Letters*, *518*, 76–85. https://doi.org/10.1016/j.epsl.2019.04.050

Molnar, P., & England, P. (1990). Late Cenozoic uplift of mountain ranges and global climate change: chicken or egg? *Nature 1990 346:6279*, *346*(6279), 29–34. https://doi.org/10.1038/346029a0

Moseley, G. E., Edwards, R. L., Wendt, K. A., Cheng, H., Dublyansky, Y., Lu, Y., et al. (2016). Reconciliation of the Devils Hole climate record with orbital forcing. *Science (New York, N.Y.)*, *351*(6269), 165–8. https://doi.org/10.1126/science.aad4132

Mulch, A., Sarna-Wojcicki, A. M., Perkins, M. E., & Chamberlain, C. P. (2008). A Miocene to Pleistocene climate and elevation record of the Sierra Nevada (California). *Proceedings of the National Academy of Sciences of the United States of America*, *105*(19), 6819–6824. https://doi.org/10.1073/pnas.0708811105

Ogg, J. G. (2020). Geomagnetic Polarity Time Scale. *Geologic Time Scale 2020*, 159–192. https://doi.org/10.1016/B978-0-12-824360-2.00005-X

Olson, K. J., & Lowenstein, T. K. (2021). Searles Lake evaporite sequences: Indicators of late Pleistocene/Holocene lake temperatures, brine evolution, and pCO2. *GSA Bulletin*. https://doi.org/10.1130/B35857.1

Olson, K. J., Guillerm, E., Peaple, M. D., Lowenstein, T. K., Gardien, V., Caupin, F., et al. (2023). Application of Brillouin thermometry to latest Pleistocene and Holocene halite from Searles Lake, California, USA. *Earth and Planetary Science Letters*, *602*, 117913.

Oster, J. L., Ibarra, D. E., Winnick, M. J., & Maher, K. (2015). Steering of westerly storms over western North America at the Last Glacial Maximum. *Nature Geoscience*, *8*(3), 201-205

Peaple, Mark D., Tierney, J. E., McGee, D., Lowenstein, T. K., Bhattacharya, T., & Feakins, S. J. (2021). Identifying plant wax inputs in lake sediments using machine learning. *Organic Geochemistry*, *156*, 104222. https://doi.org/10.1016/j.orggeochem.2021.104222

Peaple, Mark D., Bhattacharya, T., Lowenstein, T. K., McGee, D., Olson, K. J., Stroup, J. S., et al. (2022). Biomarker and Pollen Evidence for Late Pleistocene Pluvials in the Mojave Desert. *Paleoceanography and Paleoclimatology*, *37*(10), e2022PA004471. https://doi.org/10.1029/2022pa004471

Peaple, Mark D., Bhattacharya, T., Tierney, J. E., Knott, J. R., Lowenstein, T. K., & Feakins, S. J. (2023). Searles Valley Plant Wax Carbon and Hydrogen Isotopes and GDGTs during the Pliocene. https://doi.org/10.25921/cmfc-b433

Post, F. J. (1977). The microbial ecology of the Great Salt Lake. *Microbial Ecology 1977 3:2*, *3*(2), 143–165. https://doi.org/10.1007/BF02010403

Qian, S., Yang, H., Dong, C., Wang, Y., Wu, J., Pei, H., et al. (2019). Rapid response of fossil tetraether lipids in lake sediments to seasonal environmental variables in a shallow lake in central China: Implications for the use of tetraether-based proxies. *Organic Geochemistry*, *128*, 108–121.

Ravelo, A. C., Andreasen, D. H., Lyle, M., Olivarez Lyle, A., & Wara, M. W. (2004). Regional climate shifts caused by gradual global cooling in the Pliocene epoch. *Nature*, *429*(6989), 263–267.

Raymo, M. E., Kozdon, R., Evans, D., Lisiecki, L., & Ford, H. L. (2018). The accuracy of mid-Pliocene δ18O-based ice volume and sea level reconstructions. *Earth-Science Reviews*, *177*, 291–302. https://doi.org/10.1016/J.EARSCIREV.2017.11.022

Reheis, M. C., Slate, J. L., Sarna-Wojcicki, A. M., & Meyer, C. E. (1993). A late Pliocene to middle Pleistocene pluvial lake in Fish Lake Valley, Nevada and California. *Geological Society of America Bulletin*, *105*(7), 953–967.

Remeika, P., Fischbein, I. W., & Fischbein, S. A. (1988). Lower Pliocene petrified wood from the Palm Spring Formation, Anza Borrego Desert State Park, California. *Review of Palaeobotany and Palynology*, *56*(3–4), 183–198. https://doi.org/10.1016/0034-6667(88)90057-7

Rittase, W. M., Walker, J. D., Andrew, J., Kirby, E., & Wan, E. (2020). Pliocene–Pleistocene basin evolution along the Garlock fault zone, Pilot Knob Valley, California. *Geosphere*, *16*(5), 1208–1224. https://doi.org/10.1130/GES02209.1

Russell, I. C. (1885). Geological history of Lake Lahontan, a Quaternary lake of northwestern Nevada. *Monographs of the United States Geological Survey*. https://doi.org/10.3133/m11

De Schepper, S., Gibbard, P. L., Salzmann, U., & Ehlers, J. (2014). A global synthesis of the marine and terrestrial evidence for glaciation during the Pliocene Epoch. *Earth-Science Reviews*, *135*, 83–102.

Schouten, S., Hopmans, E. C., Schefuß, E., & Sinninghe Damsté, J. S. (2002). Distributional veriations in marine crenarchaeol membrane lipids: a new tool for reconstructing ancient sea water temperatures? *Earth and Planetary Science Letters*, *204*, 265–274. https://doi.org/10.1016/S0012-821X(03)00193-6

Seager, R., Ting, M., Held, I., Kushnir, Y., Lu, J., Vecchi, G., et al. (2007). Model projections of an imminent transition to a more arid climate in southwestern North America. *Science*, *316*(5828), 1181–1184.

Shackleton, N. J., & Opdyke, N. D. (1977). Oxygen isotope and palaeomagnetic evidence for early Northern Hemisphere glaciation. *Nature*, *270*(5634), 216–219.

Smith, G. I. (2009). Late Cenozoic geology and lacustrine history of Searles Valley, Inyo and San Bernardino counties, California. *US Geological Survey Professional Paper*. https://doi.org/10.3133/pp1727

Smith, G.I. (1991). Stratigraphy and chronology of Quaternary-age lacustrine deposits. *Quaternary nonglacial geology: Conterminous U.S.*, Morrison, R.B., ed., 339-352.

Smith, G. I., Barczak, V. J., Moulton, G. F., & Liddicoat, J. C. (1983). *Core KM-3, a surface-to-bedrock record of late Cenozoic sedimentation in Searles Valley, California*. *Professional Paper*. https://doi.org/10.3133/PP1256

So, R. T., Lowenstein, T. K., Jagniecki, E., Tierney, J. E., & Feakins, S. J. (2023). Holocene water balance variations in Great Salt Lake, Utah: Application of GDGT indices and the ACE salinity proxy. *Paleoceanography and Paleoclimatology, 38, e2022PA004558.* https://doi.org/10.1029/2022PA004558

Solomon, S., Plattner, G.-K., Knutti, R., & Friedlingstein, P. (2009). Irreversible climate change due to carbon dioxide emissions. *Proceedings of the National Academy of Sciences*, *106*(6), 1704–1709.

Stock, G. M., Anderson, R. S., & Finkel, R. C. (2004). Pace of landscape evolution in the Sierra Nevada, California, revealed by cosmogenic dating of cave sediments. *Geology*, *32*(3), 193–196. https://doi.org/10.1130/G20197.1

Stroup, J. S., Olson, K. J., Lowenstein, T. K., Jost, A. B., Mosher, H. M., Peaple, M. D., et al. (2023). A >200 ka U-Th Based Chronology from Lacustrine Evaporites, Searles Lake, CA. *Geochemistry, Geophysics, Geosystems*, *24*(3), e2022GC010685. https://doi.org/https://doi.org/10.1029/2022GC010685

Tan, N., Ramstein, G., Dumas, C., Contoux, C., Ladant, J.-B., Sepulchre, P., et al. (2017). Exploring the MIS M2 glaciation occurring during a warm and high atmospheric CO2 Pliocene background climate. *Earth and Planetary Science Letters*, *472*, 266–276.

Thompson, R. S. (1991). Pliocene environments and climates in the western United States. *Quaternary Science Reviews*, *10*(2–3), 115–132. https://doi.org/10.1016/0277-3791(91)90013-K

Tierney, J. E., & Tingley, M. P. (2018). BAYSPLINE: A New Calibration for the Alkenone Paleothermometer. *Paleoceanography and Paleoclimatology*, *33*(3), 281–301. https://doi.org/10.1002/2017PA003201

Western Regional Climate Center. (2022). *Cooperative Climatological Data Summaries* Retrieved from https://wrcc.dri.edu/cgi-bin/cliMAIN.pl?ca9035

Truong, C., Oudre, L., & Vayatis, N. (2020). Selective review of offline change point detection methods. *Signal Processing*, *167*, 107299. https://doi.org/10.1016/j.sigpro.2019.107299

Turich, C., & Freeman, K. H. (2011). Archaeal lipids record paleosalinity in hypersaline systems. *Organic Geochemistry*, *42*(9), 1147–1157. https://doi.org/10.1016/J.ORGGEOCHEM.2011.06.002

Wambui, G. D., Waititu, G. A., & Wanjoya, A. (2015). The power of the pruned exact linear time (PELT) test in multiple changepoint detection. *American Journal of Theoretical and Applied Statistics*, *4*(6), 581. https://doi.org/10.11648/j.ajtas.20150406.30Walker, J. D., Bidgoli, T. S., Didericksen, B. D., Stockli, D. F., & Andrew, J. E. (2014). Middle Miocene to recent exhumation of the Slate Range, eastern California, and implications for the timing of extension and the transition to transtension. *Geosphere*, *10*(2), 276–291. https://doi.org/10.1130/GES00947.1

Wang, H., Liu, W., He, Y., Zhou, A., Zhao, H., Liu, H., et al. (2021). Salinity-controlled isomerization of lacustrine brGDGTs impacts the associated MBT_{5ME}' terrestrial temperature index. *Geochimica et Cosmochimica Acta*, *305*, 33–48. https://doi.org/10.1016/J.GCA.2021.05.004

Wang, Y., Cerling, T. E., Quade, J., Bowman, J. R., Smith, G. A., & Lindsay, E. H. (1993). Stable isotopes of paleosols and fossil teeth as paleoecology and paleoclimate indicators: an example from the St. David Formation, Arizona. *Washington DC American Geophysical Union Geophysical Monograph Series*, *78*, 241–248.

Westerhold, T., Marwan, N., Drury, A. J., Liebrand, D., Agnini, C., Anagnostou, E., et al. (2020). An astronomically dated record of Earth's climate and its predictability over the last 66 million years. *Science*, *369*(6509), 1383–1387.

Western Regional Climate Center. (2013). *Cooperative Climatological Data Summaries*. Retrieved from https://wrcc.dri.edu/

Williams, A. P., Cook, E. R., Smerdon, J. E., Cook, B. I., Abatzoglou, J. T., Bolles, K., et al. (2020). Large contribution from anthropogenic warming to an emerging North American megadrought. *Science*, *368*(6488), 314–318. https://doi.org/10.1126/SCIENCE.AAZ9600

Winters, Y. D., Lowenstein, T. K., & Timofeeff, M. N. (2013). Identification of Carotenoids in Ancient Salt from Death Valley, Saline Valley, and Searles Lake, California, Using Laser Raman Spectroscopy. *Astrobiology*, *13*(11), 1065–1080. https://doi.org/10.1089/ast.2012.0952

Wu, J., Yang, H., Pancost, R. D., Naafs, B. D. A., Qian, S., Dang, X., et al. (2021). Variations in dissolved O2 in a Chinese lake drive changes in microbial communities and impact sedimentary GDGT distributions. *Chemical Geology*, *579*, 120348.

Wu, M. S., West, A. J., & Feakins, S. J. (2019). Tropical soil profiles reveal the fate of plant wax biomarkers during soil storage. *Organic Geochemistry*, *128*, 1–15. https://doi.org/10.1016/j.orggeochem.2018.12.011